

Fatigue Testing Machine Development for Microsample Evaluation of Additively Manufactured Metals

Ricardo Jorge Silva Rego

Dissertação de Mestrado

Orientador na FEUP: Prof. Dr. Joaquim Gabriel Magalhães Mendes

Orientador na UMBC: Prof. Dr. Marc Zupan



Mestrado Integrado em Engenharia Mecânica

Janeiro 2018

Resumo

O fabrico aditivo é uma tecnologia que está a revolucionar a indústria da manufatura. Apesar de não ser uma tecnologia recente, apenas nos últimos anos tem havido investimento de modo a desenvolver este tipo de fabrico.

O processo de sinterização direta por laser de metais (DMLS do inglês *Direct Metal Laser Sintering*) é um novo sistema capaz de produzir componentes de grande porte ou estruturas complexas próximas da forma final através da tecnologia de fabrico aditivo de forma totalmente automática, sem necessidade de ferramentas e diretamente baseado num modelo CAD 3D.

Nesta dissertação o desenvolveu-se um sistema para testar micro amostras à fadiga. As amostras têm dimensões de 3 mm x 250 μ m x 250 μ m (comprimento x largura x altura), produzidas por DMLS a partir de uma máquina EOS e cortadas utilizando *Electric Discharge Machining* (EDM).

A solução proposta nesta dissertação utiliza um atuador piezoelétrico para produzir a força necessária, uma célula de carga, garras capazes de suportar uma micro amostra num teste de fadiga tensão-tensão. O sistema é controlado em anel aberto por um programa de LabVIEW, desenvolvido para esta aplicação. Foi ainda ligado a um sistema de *Digital Image Correlation* (DIC) de modo a medir a deformação da amostra, bem como a formação e propagação de fraturas.

O sistema foi desenvolvido com sucesso, cumprindo os objetivos previamente definidos, nomeadamente aplicar alternadamente dois níveis de tensão até à fratura da amostra. O sistema permite ensaios de fadiga do tipo tensão-tensão, onde o tempo de ciclo varia entre os 6 e 10 segundos, dependendo da amplitude do teste. O *overshoot* é mantido dentro dos 2% dos limites máximo e mínimo de tensão desejada. Este sistema permite fazer ensaios até uma tensão máxima de 800 MPa, para as amostras descritas previamente.

Abstract

Additive Manufacturing (AM) is a technology that is revolutionizing the industry. Even though it is not a new technology, only in recent years investment was made towards developing this type of manufacturing.

Direct Metal Laser Sintering (DMLS) is an innovative system that explores the near-net shaping of large components and net shaping of small complex structures by means of AM - fully automatically, without tools and based directly on three-dimensional CAD 3D design data.

This research provides a new tool to mechanically characterize AM parts. With the goal to create a fatigue testing system capable of testing microsamples with overall dimensions of 3 mm x 250 μm x 250 μm (length x width x height), made by DMLS from an EOS machine and cut using wire Electric Discharge Machining (EDM).

The solution proposed in this dissertation uses a piezoelectric actuator to achieve the load needed, a load cell to monitor the stress values, special grips capable of holding a microsample and to perform a tension-tension fatigue test. The system is controlled by open loop LabVIEW program, coded especially for this application. A Digital Image Correlation (DIC) system was incorporated, in order to study sample strain, and crack growth and formation as well.

The system was successfully developed, achieving the planned goals, which translates to applying two stress values until sample failure. The system allows to perform tension-tension fatigue testing, with a cycle time is between 6 and 10 seconds, depending on the stress amplitude. The overshoot is kept at 2% of the desired stress limits. The maximum stress the system is able to perform is 800 MPa, using the samples mentioned previously.

Acknowledgements

I would like to first thank Dr. Marc Zupan for giving me the opportunity to work under his advisement in the Micro Materials Characterization Lab and providing me with everything I needed during this experience. Also, would like to thank Dr. Joaquim Mendes for providing assistance during this project and help me achieve this goal. This exchange would not have been possible without the help of Dr. Abel Santos, to whom I am grateful for lending his assistance and creating this amazing opportunity.

I want to thank my friends and lab mates Michael Duffy, João Santos and Ryan Carter for their tuition, good conversations, and suggestions. It was a pleasure going through this entire process of thesis writing with them and I could not be more thankful to for their help. Without their know-how and advice, I could not have finished this thesis workout. I would also like to thank my friends from FEUP and from high school who accompanied me during all these years, it was an honour going through it with them.

And finally, a thank you to the people who made me the person I am today, my father Jorge Rego, my mother Dores Silva, my sister Inês Rego and my girlfriend Regina Rodrigues.

Index

Resumo	ii
Abstract	iii
Acknowledgements	iv
Index	v
List of figures	vii
List of tables	ix
1 Introduction	1
1.1 Motivation.....	1
1.2 Aims and Scope	1
1.3 Thesis Overview	2
2 Literature review	3
2.1 Additive Manufacturing (AM)	3
2.1.1 Working Principle of Additive Manufacturing	3
2.1.2 AM system (Direct Metal Laser Sintering)	8
2.1.3 Advantages and applications of AM	9
2.2 Metal characterization	11
2.2.1 Introduction	11
2.2.2 Fatigue	11
2.2.3 Digital Image Correlation (DIC)	13
2.3 Testing systems	14
2.3.1 Microsamples and microtensile testing	14
2.3.2 Fatigue testing systems	15
3 Materials and Methods	21
3.1 Introduction.....	21
3.2 Fatigue standards	21
3.2.1 Equipment characteristics.....	21
3.2.2 Test termination.....	22
3.3 Requirements	22
3.3.1 Stress control	22
3.3.2 Frequency	22
3.3.3 Control panel	22
3.3.3 Range and type of movement	23
3.4 Equipment.....	24
3.4.1 Piezoelectric actuator.....	24

3.4.2 Load cell	27
3.4.3 I/O board.....	28
3.4.4 Extra equipment.....	28
4 Fatigue system.....	30
4.1 Introduction.....	30
4.2 Physical system.....	30
4.3 LabVIEW program	32
4.3.1 Piezoelectric actuator reset (first event)	32
4.3.2 Preload stage (second event)	32
4.3.3 Test stage (third event)	35
4.3.4 Increase/decrease load subVI	40
4.3.5 Control panel	42
4.3.6 Fatigue testing (alternating stress amplitude).....	44
5 Results and Discussion	45
5.1 Fatigue testing results	48
6 Conclusions	51
6.1 Future development and research	52
References.....	53
Appendix A: Load cell deflection	55
Appendix B: User’s manual.....	56

List of figures

Figure 1 - AM process sequence [8].....	4
Figure 2 - Flowchart of the slicing algorithm [23].....	5
Figure 3 - Left: STL file; Right: Resulting slices [23].	5
Figure 4 - Schematic of the DMLS/SLM process [2].	8
Figure 5 - Advantages overview [8].....	9
Figure 6 - Top left: turbine with cooling cavities [24]. Top right: “Optical micrograph of a CoCrMo LBMD deposit on a wrought substrate illustrating a refined carbide structure in the deposit and a small heat affected zone (HAZ)” [9]. Bottom: engine radiator [25].	10
Figure 7 – Variation of stress with time. (a) Reversed stress cycle, in which the stress alternates from a maximum tensile stress (+) to a maximum compressive stress (-) of equal magnitude. (b) Repeated stress cycle, in which maximum and minimum stresses are asymmetrical relative to the zero-stress level. (c) Random stress cycle [10]	12
Figure 8 – Tension/tension cycle graph [26].....	12
Figure 9 - Concrete sample, one big crack visible [11].....	13
Figure 10 - Concrete sample with DIC, multiple cracks visible [11].....	13
Figure 11 - DIC system.	14
Figure 12 - Schematic of weld showing transverse cross-section and longitudinal slices [12].	15
Figure 13 - Microsample locations within the weld plan view slice [12].	15
Figure 14- Left:Zwick/Roell HA series servo-hydraulic fatigue testing machine [27]; Right: Instron E1000 electric fatigue testing machine [28].....	16
Figure 15 - Cantilever load of a rotating beam [29].....	16
Figure 16 - Sample for cantilever load of rotating beam [30].....	17
Figure 17 - Cantilever type machine [31].....	17
Figure 18 – 4-point fatigue testing [31].....	18
Figure 19 - Configurations and dimensions of exemplary fatigue samples [32].....	19
Figure 20 - Standard sample mounted on test machine[27].	19
Figure 21 - Microsamples stress/strain curves (a) generic steel [33]; (b): Ti-5111 welded [12].	23
Figure 22 - System architecture.	24
Figure 23 - Example of a piezo stack actuator (1 Case, consisting of: 1a: Base with wrench flat 1b: Case tube; 2 Moving pusher with wrench flat and M8 internal thread; 3 Cable exit for piezo voltage; 4 Protective earth connection) [18].....	25
Figure 24 - Longitudinal displacement (top) and polarization of the individual layers (bottom) of a stack actuator [18].	25
Figure 25 - E-508.00 amplifier module [18].	26
Figure 26 – (a): Festo short stroke actuator [34]; (b) Voith hydraulic actuator system [35]; (c) Tolomatic rod-style linear actuator [36].....	26

Figure 27 - Wheatstone bridge with load cell wiring [20].	27
Figure 28 - DPM-3 Digital Panel Mount Load Cell Meter [20].	27
Figure 29 - National Instruments USB-6211 I/O device [37].	28
Figure 30 - (a) Newport picomotor [38]; (b) Linear stage.	28
Figure 31 - Air bearing (Top: ISO view; Bottom: Cross section) [39].	29
Figure 32 - Fatigue testing system (top view).	30
Figure 33 - Fatigue testing system (side view).	31
Figure 34 - Grips with sample (top view).	31
Figure 35 - Grips with sample (lateral view).	32
Figure 36 - Preload stage.	34
Figure 37 - Max cycles subVI.	36
Figure 38 - Serial communication read code.	37
Figure 39 - Test stage.	38
Figure 40 - Test stage.	39
Figure 41 - Increase/decrease load subVI.	41
Figure 42 - Control panel.	43
Figure 43 - Block counter subVI.	44
Figure 44 - Stress/time graph fatigue testing.	47
Figure 45 - Stress-time graph of alternating stress amplitude.	48
Figure 46 - Z ₃₄ (core) fracture 1000x.	50
Figure 47 - Z ₃₅ (core) fracture 1000x.	50
Figure 48 - Z (skin) fracture 1000x.	50
Figure 49 - Stay rod representation [22].	55

List of tables

Table 1 - AM processes and equipment manufacturers [2].....	7
Table 2 - Stress/load values for cantilever testing.....	17
Table 3 - Stress/load values for 4-point testing.....	18
Table 4 - Fatigue testing results.....	49

1 Introduction

The present dissertation was developed and submitted to the Faculdade de Engenharia da Universidade do Porto (FEUP) in partial fulfillment of the requirements for the degree of Master of Science in Mechanical Engineering. The research project was developed at the University of Maryland Baltimore County (UMBC).

1.1 Motivation

While the rapid evolution of Additive Manufacturing (AM) has promoted numerous innovative processes and machines, AM has grown with minimal understanding of the impact of processing parameters on global part properties making it difficult for industry to take full advantage of the technology. The layer-by-layer approach used by almost all AM machines to build these novel parts has direct definite ramifications for the microstructures and mechanical properties of these parts. Despite the recent interest in additive manufacturing, the property variations are still not fully known neither understood. This is because conventional mechanical characterization techniques usually measure an average property and cannot resolve the important variations tied to specific microstructural features present in the sample nor are capable to differentiate the anisotropic properties of this type of parts.

1.2 Aims and Scope

The aim of this work is to develop a system for fatigue and fatigue life characterization in small samples built by AM. Microtensile testing, conducted at UMBC, allows one to accurately and effectively probe the mechanical properties of materials of interest on the local level. Microtensile specimens with overall dimensions of 3mm x 1mm with ~0.30 mm square gage section can be extracted from microstructural areas of interest in the additively manufactured materials.

Aiming to expand the testing capabilities available at the micromaterials laboratory at UMBC, in this project, the scope is to build a microtensile tester to operate in fatigue. The machine will be composed of wedge grips, a load cell, a piezoelectric stack and correspondent controller. A LabVIEW user interface should be developed to monitor and control the system, where it is possible to control the frequency of testing, upper and lower load limits, and all safety controls and user interface as well. Each component of the testing system will meet the unique challenges of microsample testing. The novel testing system will be utilized to characterize newly additively manufactured alloys, specifically AlSi10Mg aluminum alloy manufactured using direct metal laser sintering from an Electro Optical Systems (EOS) machine.

1.3 Thesis Overview

Chapter 2 consists of a review of relevant studies important to frame this work. In the review, a brief introduction to the Additive Manufacturing (AM) process will be made, in which different systems will be mentioned, with special attention to the Direct Metal Laser Sintering system. Afterwards, metal characterization is explained, with focus on fatigue, Digital Image Correlation and microsamples, all based on peer-reviewed published papers.

Chapter 3 discusses the methods used, requirements and expectations for this dissertation.

Chapter 4 presents the system built, including equipment setup and LabVIEW code written, while explaining the process behind it.

Chapter 5 is the discussion of the solution, how components work with each other, the logic behind the program and how problems were overcome.

Finally, chapter 6 discusses the conclusions that can be drawn and the future work to continue the research forward.

2 Literature review

2.1 Additive Manufacturing (AM)

AM is defined by the American Society for Testing and Materials (ASTM) as the “...process of joining materials to make objects from 3D model data, usually layer upon layer, as opposed to subtractive manufacturing methodologies...” [1]. It is also known as additive fabrication, additive process, additive technique, rapid manufacturing and 3D printing [1].

Originally called rapid prototyping, AM was developed as a cost-effective and time-efficient way to produce a prototype for design. However, due to the driving force from industry to seek for innovation in materials and processes, AM has changed from prototype production to rapid manufacturing. Since its inception in the mid-1980s, AM has evolved and blossomed into a whole range of processes, those are summed up in Table 1 [2].

2.1.1 Working Principle of Additive Manufacturing

AM technology follows a different path when compared with subtractive manufacturing, the AM process includes the following steps as shown in Figure 1.



Figure 1 - AM process sequence [8].

The steps 1, 2 and 5 are common to subtractive processes based on Computer Numerical Control (CNC). The STL file (originally created by 3D Systems Inc. when they first developed the stereolithography) that is used vastly in CNC fabrication, "...converts the continuous geometry in the CAD file into a header, small triangles or coordinates triplet list of x, y and z coordinates and the normal vector to the triangles..." [3].

A piece manufactured by AM is built layer upon layer, so it is needed to convert the solid geometry of a CAD file into layers. For the slicing step, a flowchart, shown in Figure 2, was designed to generate the best slice's orientation and the way the part is going to be built.

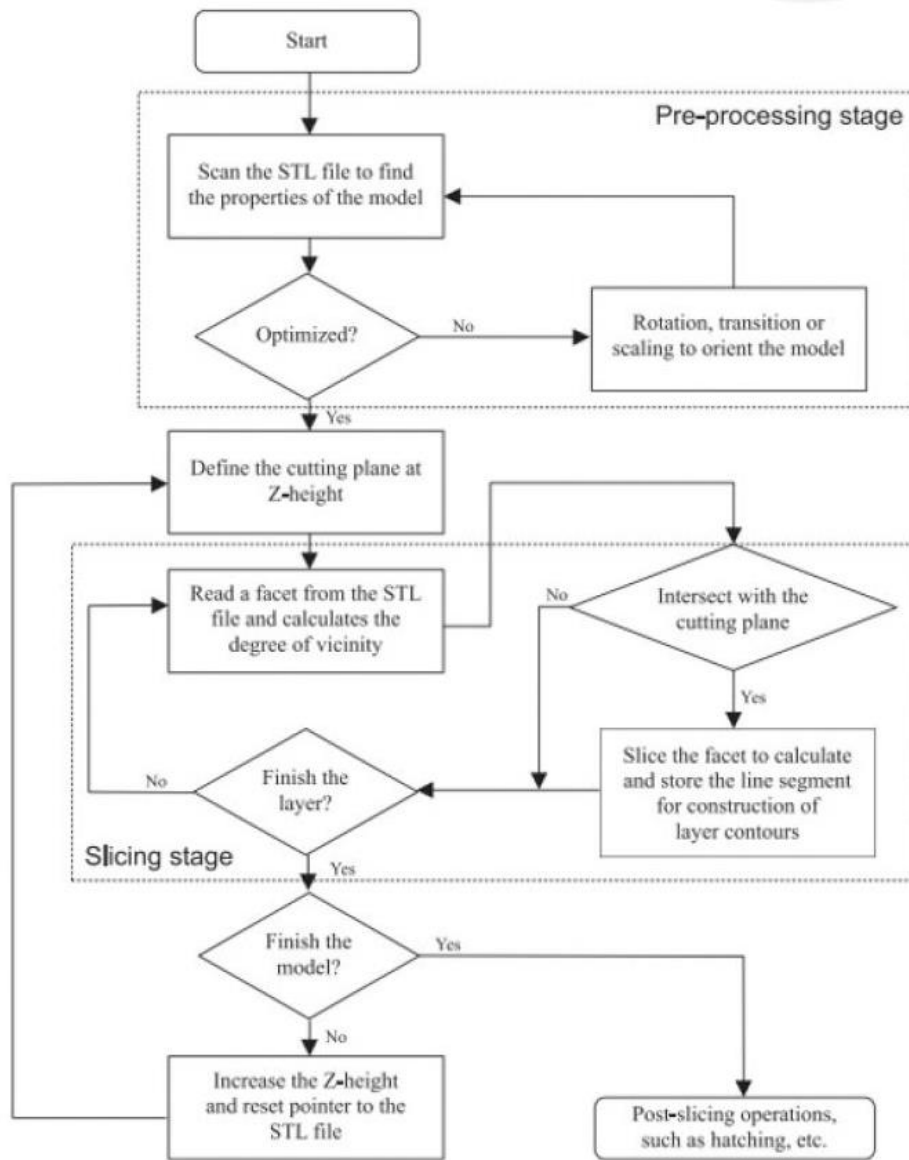


Figure 2 - Flowchart of the slicing algorithm [23].

After the slicing process, a slice file is generated, as shown in Figure 3.

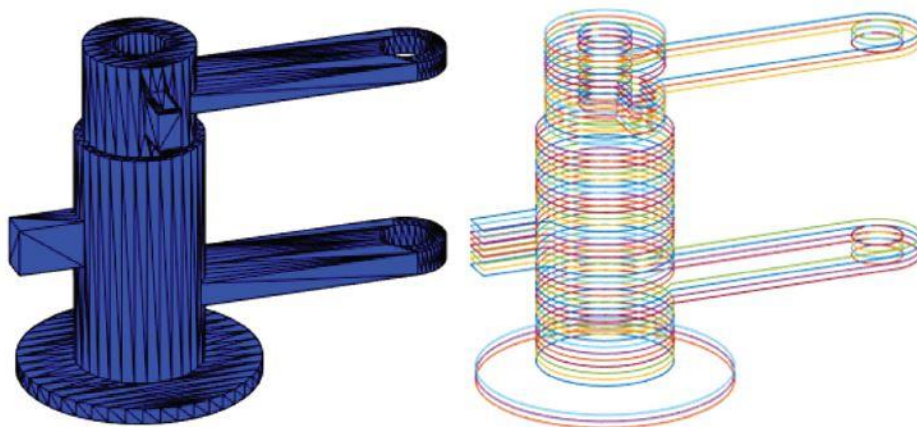


Figure 3 - Left: STL file; Right: Resulting slices [23].

After obtaining the slices file, the next step is building the part in the selected AM system. Many processes are available (Table 1), each one with different properties, suitable for different materials and geometries. The system of interest for this project is explained on the sub-chapter 2.1.2 AM system (Direct Metal Laser Sintering).

In metal AM technology, parts are not ready for end-use applications directly out of a machine, so the step 5 of Figure 1 as to be performed. There are many steps that are typically used to prepare an as-fabricated part into an end-use part, including excess powder removal, build substrate and support structures removal, thermal treatments to improve mechanical behaviour, and surface finishing to achieve desired geometrical tolerance and surface finish [4]. After a part is done, excess powder, support structures and substrate material must be removed and stress relief must be performed. Stress relief involves recovery. Atomic diffusion increases at elevated temperatures, and atoms in regions of high stress can move to regions of lower stress, which results in the relief of internal strain energy. SLM and DMD parts are usually annealed to remove residual stress, commonly prior to substrate removal [4].

Table 1 - AM processes and equipment manufacturers [2].

Process Category	Process/Technology	Material	Manufacturer(s)
Vat photopolymerization	SLA (Stereolithography)	UV curable resins	Asiga
			3D Systems
		Waxes	Envision TEC
			Rapidshape
Material jetting	MJM (Multi-Jet Modeling)	UV curable resins	DWS
			Lithoz
		Waxes	3D Systems
			Stratasys
Binder jetting	3DP (3D printing)	Composites	Solidshape
			3D Systems
		Polymers,Ceramics	Voxjet
			Metals
Material Extrusion	FDM (Fused Deposition Modeling)	Thermoplastics	Stratasys
			MakerBot
		Waxes	RepRap
			Bits from Bytes
		Thermoplastics	Fabbster
			Delta Micro Factory Corporation
		Metals	Beijing Tiertime
			ChocEdge
		Waxes	Essential Dynamics
			Fab@Home
Powder bed fusion	SLS (Selective Laser Sintering)	Thermoplastics	EOS
			Blueprinter
		Metals	3D Systems
			3Geometry
			Matsuura
	SLM (Selective Laser Melting)	3D Systems	
		Metals	EOS
		SLM Solutions	
		Concept Laser	
		3D Systems	
EBM (Electron Beam Melting)	Metals	Realizer	
		Renishaw	
	Metals	Arcam	
		Sciaky	
Sheet lamination	LOM (Laminated Object Manufacturing)	Paper	Mcor Technologies
		Metals	Fabrisonic
		Thermoplastics	Solido
Direct energy deposition	LMD/LENS (Laser Metal Deposition)	Metals	Optomec
			Dm3D
	EBAM (Electron Beam AM)	Metals	Irepa Laser
			Sciaky

2.1.2 AM system (Direct Metal Laser Sintering)

As mention in the previous section, there are numerous solutions to manufacture a part. In this sub-chapter, it will be explained the system used to produce the parts which the samples will be taken from.

Direct Metal Laser Sintering (DMLS) is a type of powder bed fusion system developed by EOS. Metal powder bed fusion AM system, represented in Figure 4, is “an additive manufacturing process in which the thermal energy selectively fuses regions of a powder bed” [5]. In this type of metal AM process, thin layers of powder are applied to a build plate and an energy source (laser or electron beam) is used to fuse the powder contained in a bed [5]. The system is composed of a powder delivery system, an energy delivery system and two beds of powder: one where the part is built and one holding the reserve powder. The powder delivery system comprises a feeding system, a spreader, and a piston. The energy delivery system is made up of a laser and a scanner system that enables the delivery of a focused spot to all points of the build platform [5, 6].

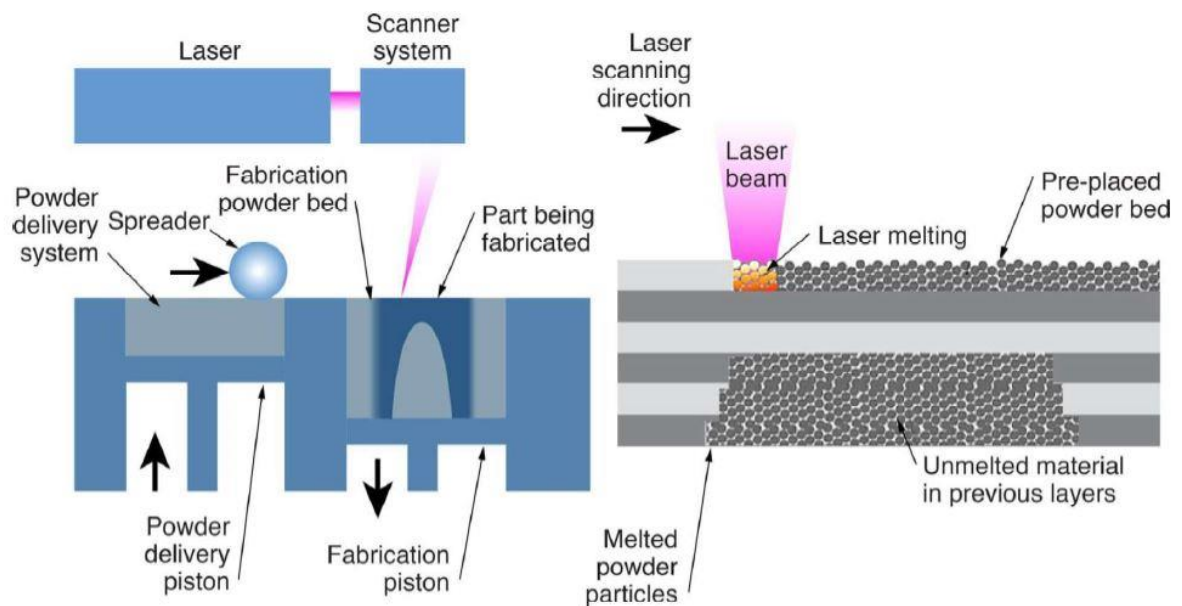


Figure 4 - Schematic of the DMLS/SLM process [2].

2.1.3 Advantages and applications of AM

AM has been developed since the 1980's, due to its economic advantages and a wide range of applications.

Economically, being an additive technology, it is possible to get a Buy-to-Fly ratio⁽¹⁾ close to 1 and as a direct consequence, the waste is reduced to 10-20%, which results in a decrease of the part cost by 50% [8]. On the technical side, AM allows the design of complex parts with intricate geometries, that with conventional methods of manufacturing would not be possible [3, 6]. Also, AM allows a level of mass customization, meaning it is possible to produce a somewhat large quantity of products, different from each other. For large quantities, it is still more profitable to use more standard manufacturing methods.

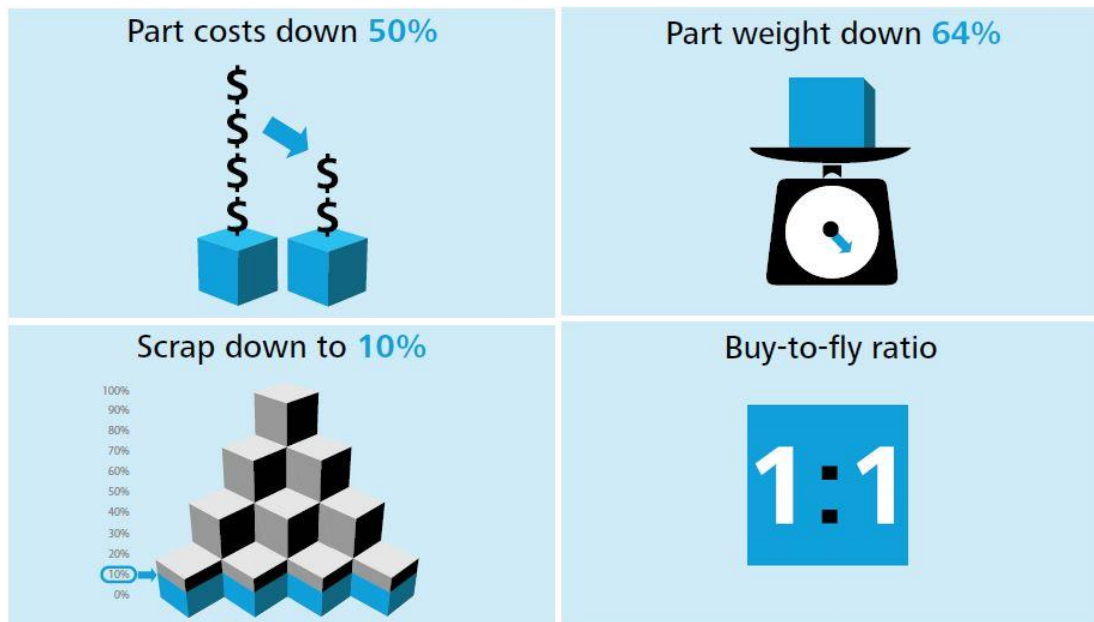


Figure 5 - Advantages overview [8].

(1) Buy-to-Fly ratio is the ratio between the weight of the raw material and the weight of the finalized part.

Thanks to all the advantages discussed previously, a vast set of areas are interested in this technology. For example, the aerospace industry is a sector that it is known for the complex forms and geometries, made of advanced materials. As seen in Figure 6 (top left), AM allows the fabrication of voids in a part, for example, cavities to allow airflow inside a turbine.

The automotive industry is another big market for AM, as shown in Figure 6 (bottom).

Another sector with direct impact on people’s lives is the biomedical area. Laser-Based Metal Deposition (LBDM) “LBMD processes are a subset of additive manufacturing processes that enable the deposition of various metal powders onto substrate geometries” [9], this allows the combination of different alloys in specific areas, and as a consequence have localized mechanical properties.



Figure 6 - Top left: turbine with cooling cavities [24]. Top right: “Optical micrograph of a CoCrMo LBMD deposit on a wrought substrate illustrating a refined carbide structure in the deposit and a small heat affected zone (HAZ)” [9]. Bottom: engine radiator [25].

2.2 Metal characterization

2.2.1 Introduction

“Many materials, when in service, are subjected to forces or loads; examples include the aluminum alloy from which an airplane wing is constructed and the steel in an automobile axle. In such situations, it is necessary to know the characteristics of the material (...) The mechanical behavior of a material reflects the relationship between its response or deformation to an applied load or force.” [10]. Mechanical properties are a set of data that allows the user to comprehend the behavior of a material.

“The mechanical properties of materials are ascertained by performing carefully designed laboratory experiments that replicate as nearly as possible the service conditions. Factors to be considered include the nature of the applied load and its duration, as well as the environmental conditions.” [10].

Metal characterization is the process to determinate, through various tests, the mechanical properties of the metal, properties such as tensile/compressive stress, strain, elastic properties, yield strength, hardness and fatigue life.

2.2.2 Fatigue

“Fatigue is a form of failure that occurs in structures subjected to dynamic and fluctuating stresses (...). Under these circumstances, it is possible for failure to occur at a stress level considerably lower than the tensile or yield strength for a static load.” [10].

Fatigue is the largest cause of failure in metals, estimated to comprise approximately 90% of all metallic failures [10], and occurs suddenly and without warning. Fatigue failure is brittlelike in nature, which means that there is very little, or none, plastic deformation associated with failure [10].

Fatigue testing consists of applying a cyclic stress (axial/flexural/torsional) to a sample until it breaks (fails). The majority of tests apply one of three stress cycles, see Figure 7.

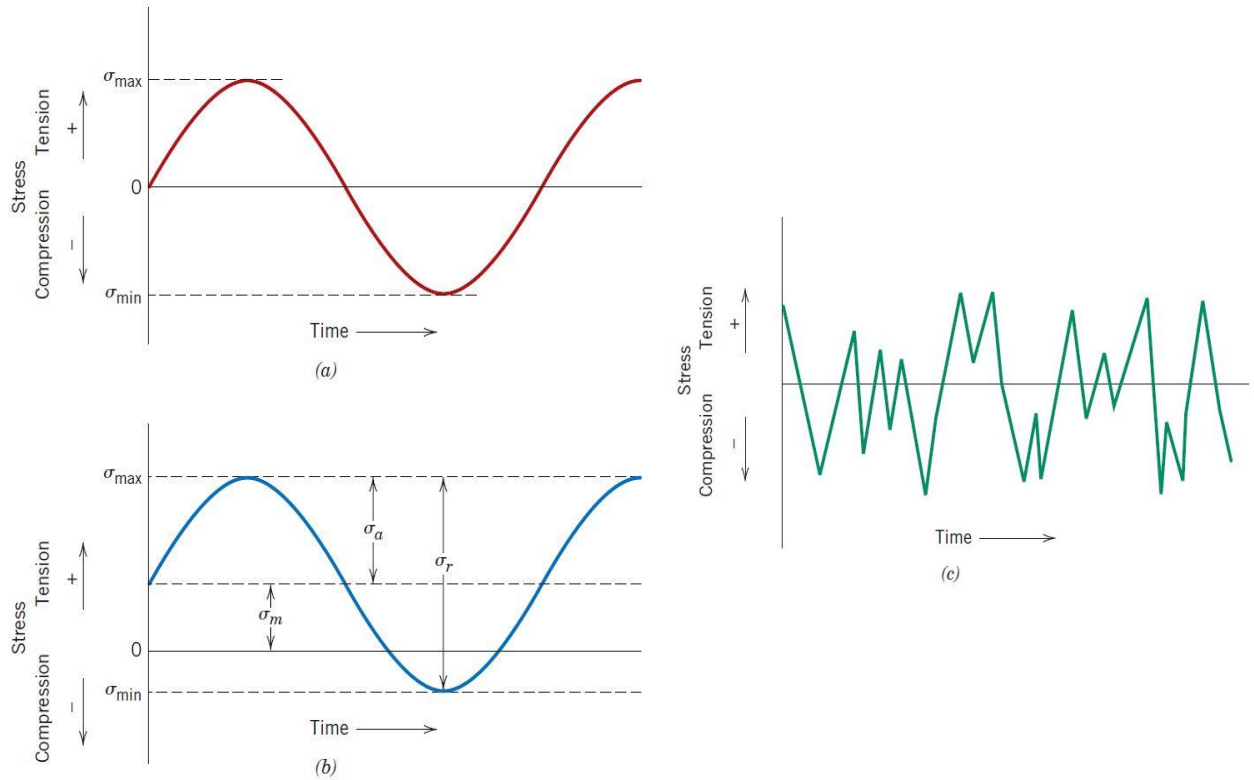


Figure 7 – Variation of stress with time. (a) Reversed stress cycle, in which the stress alternates from a maximum tensile stress (+) to a maximum compressive stress (-) of equal magnitude. (b) Repeated stress cycle, in which maximum and minimum stresses are asymmetrical relative to the zero-stress level. (c) Random stress cycle [10]

In this project, a fourth stress cycle will be applied, Figure 8. This one is called tension/tension cycle, this means throughout the cycle, only tension is applied, $\sigma_{\min} > 0$. From this graph, we obtain the ratio $R = \sigma_{\min} / \sigma_{\max}$, R will be a requirement in Chapter 3.

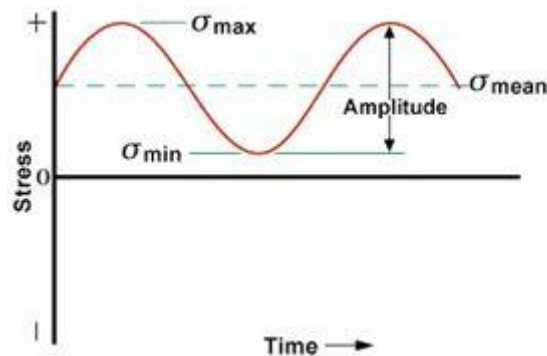


Figure 8 – Tension/tension cycle graph [26].

2.2.3 Digital Image Correlation (DIC)

“Digital Image Correlation (DIC) is an innovative non-contact optical technique for measuring strain and displacement. DIC is simple to use and cost-effective compared to other techniques (...). DIC works by comparing digital photographs of a component or test piece at different stages of deformation. By tracking blocks of pixels, the system can measure surface displacement and build up full field 2D and 3D deformation vector fields and strain maps.” [11].

This system (Figure 11) is easy to operate and can be controlled using a LabVIEW program. It is used to study crack tip and crack propagation.

DIC is a tool to characterize a material, to better understand its behavior under certain conditions. At the micromaterials lab, this technique is used with microsample tensile testing and can be adapted to the fatigue testing system.

The results of using this tool can be seen in Figure 9 and Figure 10.



Figure 9 - Concrete sample, one big crack visible [11].

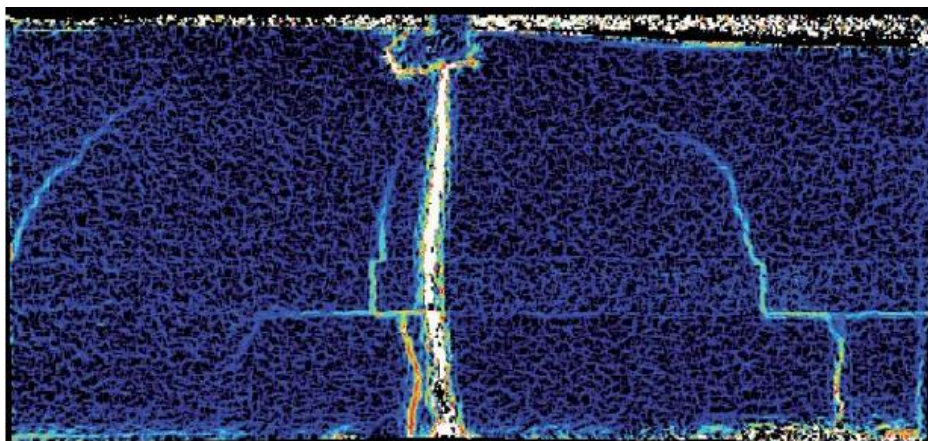


Figure 10 - Concrete sample with DIC, multiple cracks visible [11].

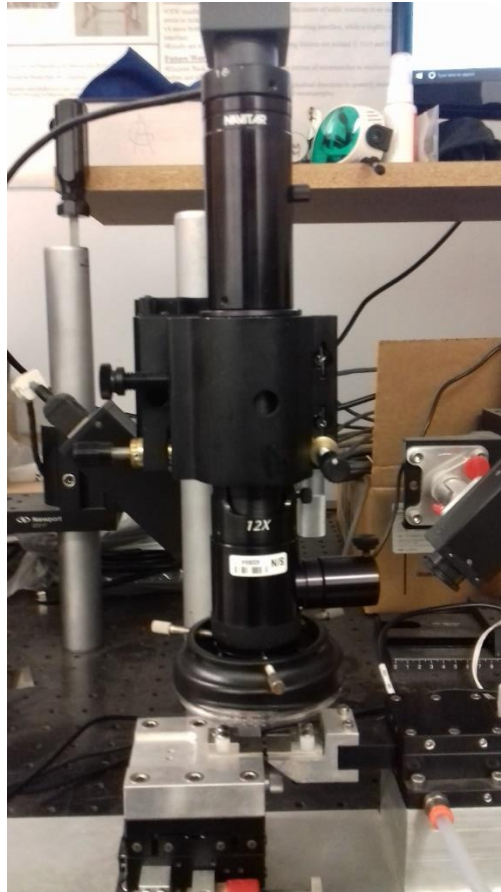


Figure 11 - DIC system.

2.3 Testing systems

To determine a mechanical property, a sample of the material as to be subjected to a test in a controlled environment and with repeatable/controllable test parameters.

2.3.1 Microsamples and microtensile testing

Conventional mechanical characterization techniques usually measure an average property and cannot resolve the important variations tied to specific microstructural features present in the sample. In order to get a more local analysis, resorting to testing microsamples can help to understand the local mechanical properties.

The small-scale samples are prepared by slicing the material to a thickness of 1 mm, using wire electric discharged (EDM) [12]. After EDM, each slice is polished to mitigate any machining effects [12]. To get the mechanical test samples, sinking EDM with graphite electrode is used to extract the microsamples (3 mm x 1 mm footprint with a 250 μm x 250 μm gage area) (Figure 12 and Figure 13) [12].

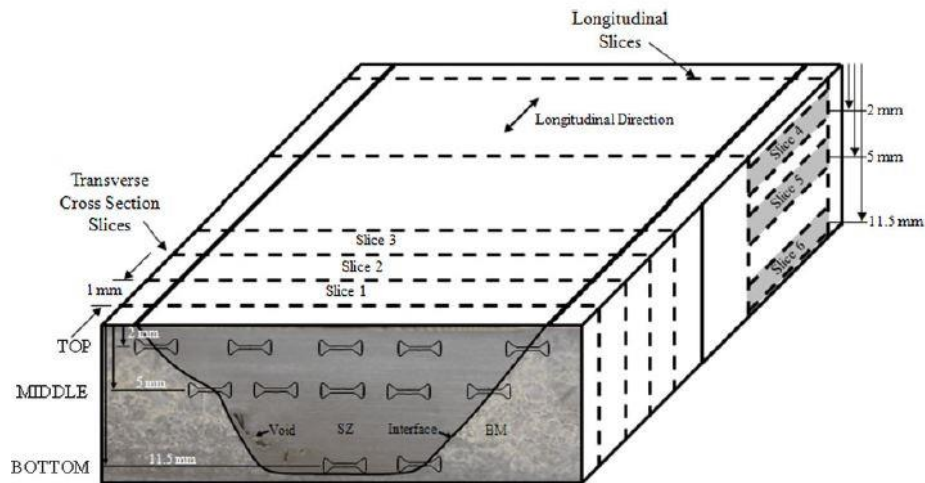


Figure 12 - Schematic of weld showing transverse cross-section and longitudinal slices [12].

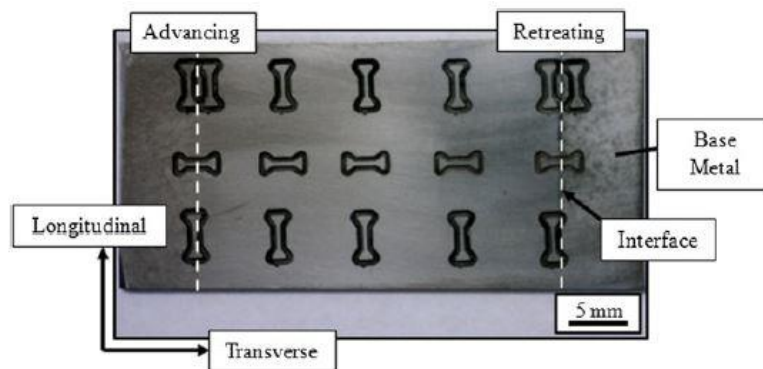


Figure 13 - Microsample locations within the weld plan view slice [12].

This sample geometry has a proven effect on measuring the mechanical properties of a variety of materials [12–14].

At the micromaterials lab at UMBC, microtensile testing is currently being done to evaluate the mechanical properties of several metal alloys made using AM technology.

2.3.2 Fatigue testing systems

There is a wide range of commercial fatigue testing systems, all-electric, hydraulic or servo-electric are just a few of the options. These systems are comprised of a hydraulic piston or electric motor, grips made for the standard round or flat samples (Figure 19), load cells and control panels.

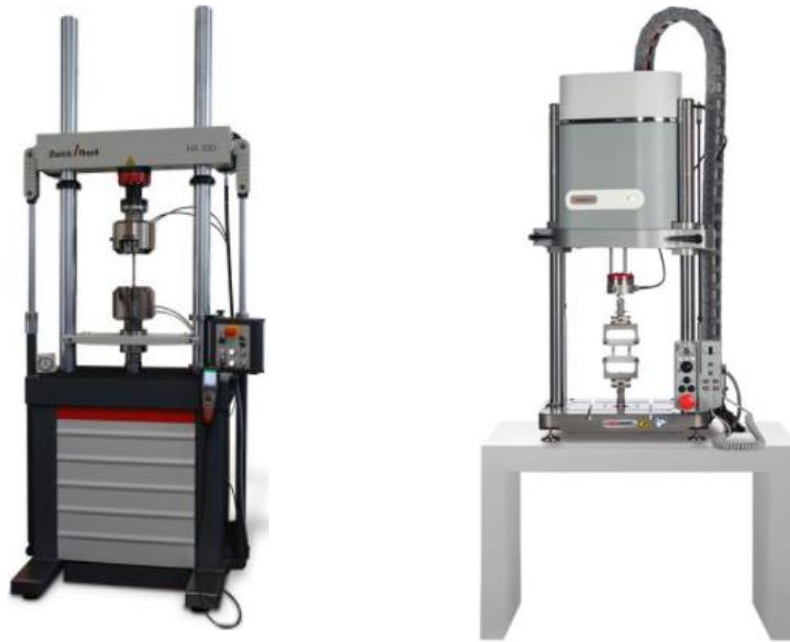


Figure 14- Left:Zwick/Roell HA series servo-hydraulic fatigue testing machine [27]; Right: Instron E1000 electric fatigue testing machine [28].

In Figure 14, two examples are shown. What both commercial systems available have in common is the high dynamic linear force capacity (1 kN for the Instron system and 50 kN for the Zwick/Roell) and the long linear stroke (minimum 60 mm for the Instron system). This means that commercial systems are aimed at macro testing and therefore not suitable for micro testing.

In order to answer to the need of localized mechanical characterization that has arisen from the interest in AM technology, microsamples testing systems were developed thus the goal of this dissertation.

Another system, that is able to test at high frequencies is the cantilever loading of a rotating beam (Figure 15).

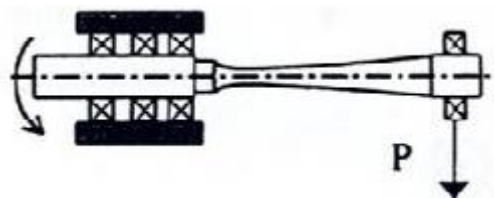


Figure 15 - Cantilever load of a rotating beam [29].

In this system, a beam rotates using a motor, while a constant load is being applied at one end, this means that a section of the sample is constantly alternating between tension and compression (R value of -1). The central section of a sample (Figure 16) is under an alternating stress of constant amplitude (Figure 7a), the amplitude is controlled by the value of the mass hanging at the end of the sample. The advantage of this system is the high frequency.

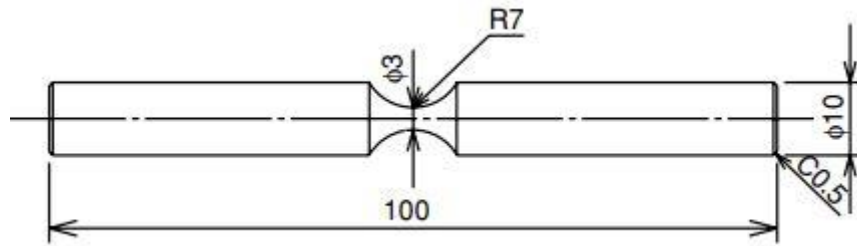


Figure 16 - Sample for cantilever load of rotating beam [30].

Trying to adapt a system of this kind to microsample testing requires analysing this solution mathematically, to try understanding what values of load are in play to reach the desired stress.

In a standard cantilever type machine (Figure 17), the stress in the sample is given by equation 2.1, and simplifying it to the shape of a sample as the one in Figure 16, the result is equation 2.2.

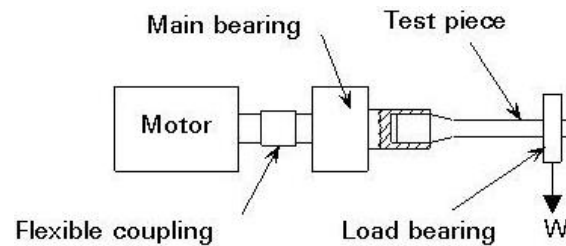


Figure 17 - Cantilever type machine [31].

Defining the microsample with 3 mm in length and 250 μm in diameter, the point of maximum stress is the middle of the sample ($x = 1.5 \text{ mm}$) and applying this values to equation 2.2, the load results are represented in Table 2.

Table 2 - Stress/load values for cantilever testing.

Stress [MPa]	Load [N]	Mass [g]
100	0.205	20.8
150	0.307	31.3
200	0.409	41.7
250	0.511	52.1
300	0.614	62.5

Another type of rotating machine uses the 4-point bending method (Figure 18). In this machine, the bending moment is given by equation 2.3.

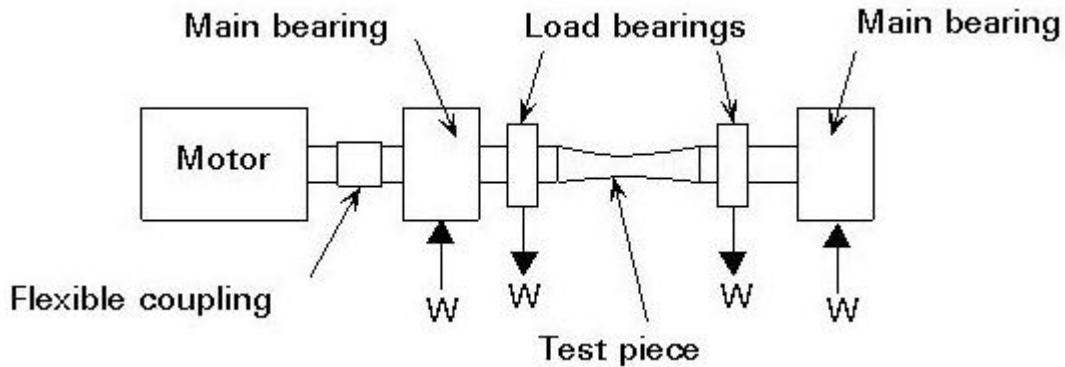


Figure 18 – 4-point fatigue testing [31].

Defining the microsample with 13 mm (5 mm between main and loading bearing) in length and 250 μm in diameter and applying this values to equation 2.4, the load results are the represented in Table 3.

Table 3 - Stress/load values for 4-point testing.

Stress [MPa]	Load [N]	Mass [g]
100	0.12	12.5
150	0.18	18.8
200	0.25	25.0
250	0.31	31.3
300	0.37	37.5

Granted that some considerations regarding the shape and the size of the sample were made, the load values are possible to achieve but many times greater than the weight of the sample. The problem with rotating testing being the size of the sample comparing to the system another problem related to a system that could perform this test would be the requirement of a lot of custom parts. Also, producing a cylindrical micro sample would require high precision machining and as results, the cost would increase considerably while using wire EDM to produce the flat samples that are already being used only requires polishing post-processing that can be done at the micromaterials lab.

Looking at what is currently available in the market, a system capable of performing the type of testing desired was not found.

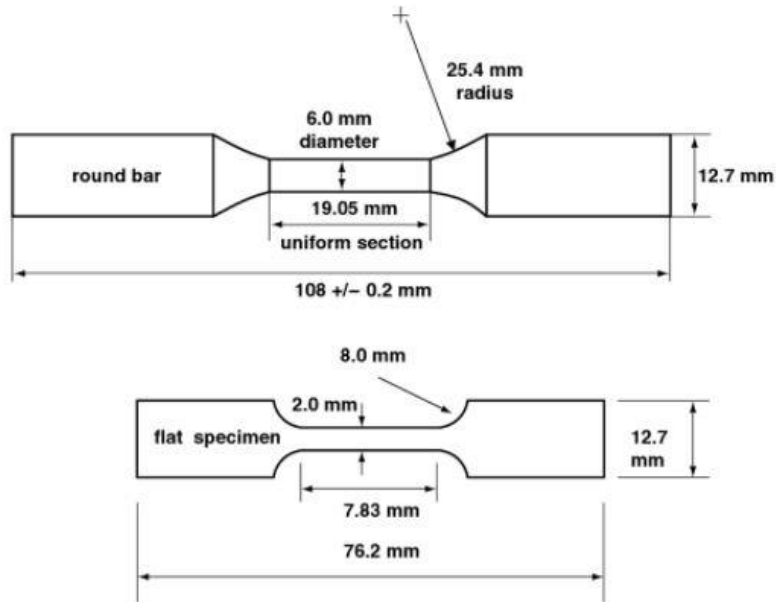


Figure 19 - Configurations and dimensions of exemplary fatigue samples [32].



Figure 20 - Standard sample mounted on test machine[27].

$$\sigma = \frac{M_f \times y}{I} \quad (2.1)$$

Where:

σ , is stress

M_f , is bending moment

y , is the distance of a point to the neutral axis

I , is the polar momentum of inertia

$$\sigma = \frac{W \times (l-x) \times \frac{d}{2}}{\frac{\pi \times d^4}{32}} \quad (2.2)$$

Where:

W , is applied load

l , is the length of the sample

x , is the distance from the load to the point desired

d , is the diameter

$$M_f' = W \times a \quad (2.3)$$

Therefore:

$$\sigma = \frac{W \times a \times \frac{d}{2}}{\frac{\pi \times d^4}{32}} \quad (2.4)$$

Where:

M_f' , is the bending moment in the test piece

W , is applied load

a , is the distance between the main bearing and the load bearing next to it

3 Materials and Methods

3.1 Introduction

This section is dedicated to presenting the problem at study, explaining what is required and what is available to work with and the system specifications as well.

3.2 Fatigue standards

Depending on the type of control desired for the testing there is a respective ASTM standard. The movement is controlled using the stress variable set point, according to the ASTM E466-15 “Standard Practice for Conducting Force Controlled Constant Amplitude Axial Fatigue Tests of Metallic Materials” (ISO 1099:2017 “Metallic materials - Fatigue testing - Axial force-controlled method”). The available standard is E466-96 (which is the previous version of the E466-15) and can be used as a guideline for this project. This standard [15] also specifies specimen design, specimen preparation, but for this project the sections that matter are equipment characteristics and test termination.

3.2.1 Equipment characteristics

Following the E466-96 standard, it is explained that the test machines should have a force-monitoring system and the test forces should be monitored continuously in the early stage of the test and periodically, thereafter [15]. In this case, the force transducer is the load cell mentioned in section 3.4.2 Load cell. Regarding the stress amplitude, it should be maintained at all times within 2% of the desired test value [15]. The test Frequency is typically in the regime of 10^{-2} to 10^{+2} Hz but fatigue strength is generally unaffected (by the test frequency) for most metallic engineering materials [15].

3.2.2 Test termination

The test should be finalized either if the specimen failure criteria are attained, or if a predetermined number of cycles has been applied to the specimen [15].

3.3 Requirements

The requirements for the system are first and foremost reliability, this means that the program must run uninterrupted until the test termination parameters (section 3.2.2 Test termination) are obtained. Other requirements are further explained in the next sections.

3.3.1 Stress control

Stress control means that constant displacement is applied, while force is monitored, to the sample until it reaches the maximum stress value selected by the user, and then applies constant displacement until the minimum stress value selected by the user is reached and repeating until the test termination parameters are achieved.

3.3.2 Frequency

The frequency requirement, based on the ASTM standards (section 3.2.1 Equipment characteristics) is between 10^{-2} and 10^{+2} Hz, although the testing frequency should be such that the overshoot is reduced to the minimum value possible.

3.3.3 Control panel

The control panel is the user interface, as such must have value inputs (maximum/minimum stress values, maximum number of cycles, cross-sectional area), outputs (stress graph, stress value display, cycles complete value display, sample failure indicator, maximum number of cycles reached indicator) and control buttons (preload stage, start test, reset piezo actuator and stop), plus any others that may be necessary.

3.3.3 Range and type of movement

A starting point to decide what type of actuator to choose is to perform an analysis of the movement required to create the stress desired on the sample.

It has been established in the section 2.3.2 Fatigue testing systems, that rotating cantilever is not possible to use with the type of samples in the study, therefore linear movement is required.

High cycle fatigue is the type of fatigue that will be determined with this system. This type of fatigue is characterized by performance in the elastic region (as opposed to low cycle fatigue that performs in the plastic region [16]) and with a high value of cycles reached [17]. With this in mind, it is possible to determine the displacement required by performing a tensile test on a microsample and find the yield point and correspondent strain value.

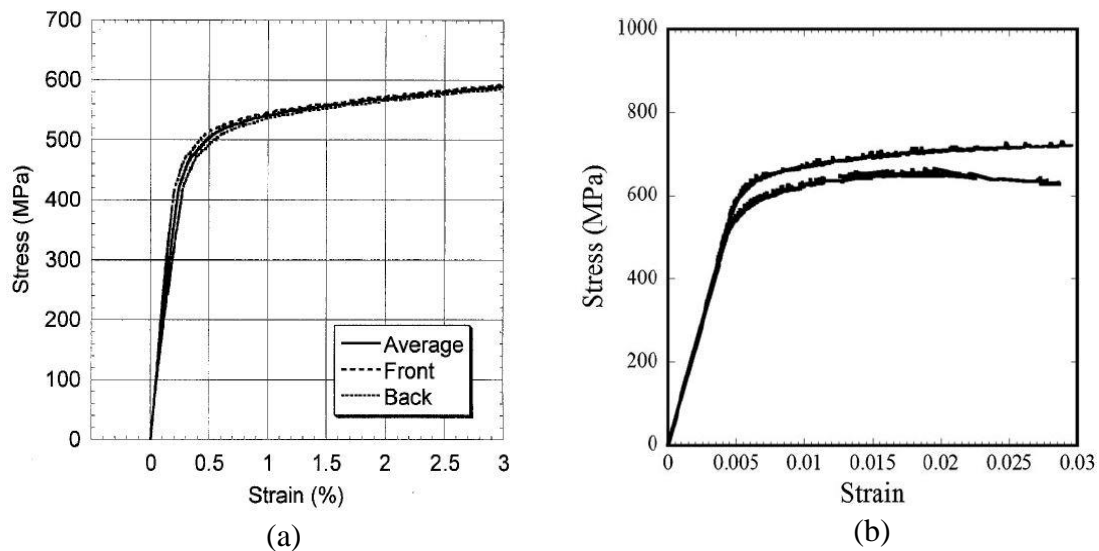


Figure 21 - Microsamples stress/strain curves (a) generic steel [33]; (b): Ti-5111 welded [12].

Looking at the two examples of Figure 21, it can be noted that the yield strain value is below 0.5%. Both samples were 3 mm in length, therefore the maximum displacement was 15 μm .

3.4 Equipment

As said previously, the system is composed of a piezoelectric actuator, a load cell, grips, following the system architecture shown in Figure 22.

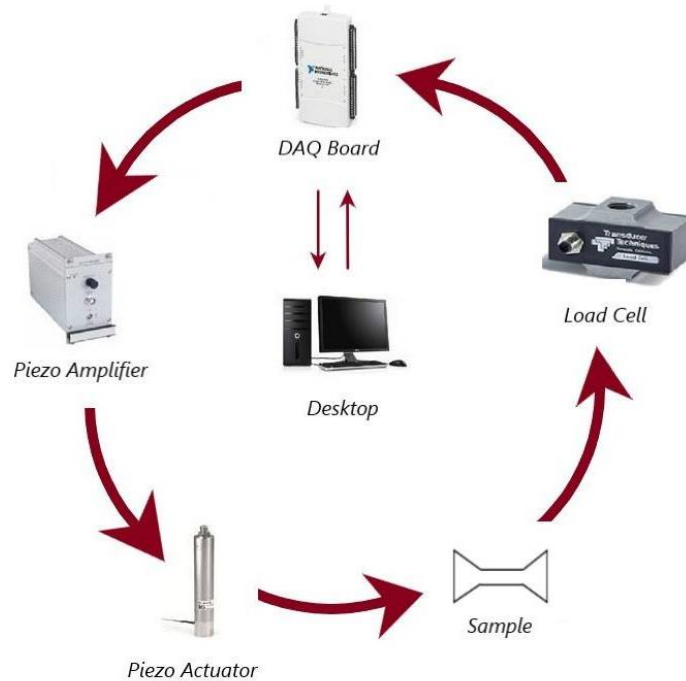


Figure 22 - System architecture.

3.4.1 Piezoelectric actuator

The piezoelectric actuator is a linear actuator based on the inverse piezoelectric effect [18]. “In longitudinal piezo actuators, the electric field in the ceramic layer is applied parallel to the direction of polarization. This induces a strain or displacement in the direction of polarization. Individual layers give relatively small displacements. In order to achieve technically useful displacement values, stack actuators are constructed, where many individual layers are mechanically connected in series and electrically connected in parallel.” [18] (Figure 24).

“Longitudinal stack actuators are excellently suited for highly dynamic operation due to their high resonant frequencies.” [18], therefore the piezoelectric actuator available at the micromaterials lab is ideal for the system.

The actuator available is a Physik Instrumente (PI) P-239.90 (Figure 23), it is a longitudinal stack actuator with the following specifications [19]:

- Travel range to 180 μm ;
- Pushing/Pulling forces of 4500/500 N;
- Sub-ms response;
- Open loop resolution 1.80 nm;

This piezo actuator is paired with an amplifier in this case, is the E-508.00 piezo amplifier module (Figure 25). This module as an output voltage of 1100 V and allows the piezo actuator to be controlled by a computer using an I/O board that outputs 0-10V DC.



Figure 23 - Example of a piezo stack actuator (1 Case, consisting of: 1a: Base with wrench flat 1b: Case tube; 2 Moving pusher with wrench flat and M8 internal thread; 3 Cable exit for piezo voltage; 4 Protective earth connection) [18].

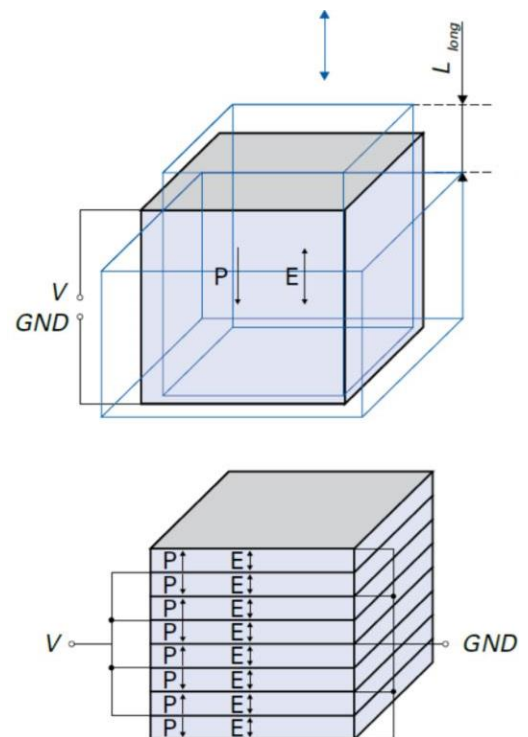


Figure 24 - Longitudinal displacement (top) and polarization of the individual layers (bottom) of a stack actuator [18].



Figure 25 - E-508.00 amplifier module [18].

To justify why the piezoelectric actuator is the best option, it is needed to look at what is available in the market.

One option is pneumatic actuators (Figure 26 a), even though short stroke actuators are available, precision positioning is not the main goal of these actuators, being optimized to move to each stroke end. Hydraulic actuators (Figure 26 b) are design to heavy duty operations and require an intricate system of hydraulic pump and electric motor therefore not suitable for this application.

Another solution is electric driven actuators. There are a few types of actuators powered by electric motors such as rod-style, screw-driven, magnetic and others. Screw-driven actuators are designed to move moderate to heavy loads and therefore not optimize for the type of application in this system. Traditional rod-style actuators have strokes inappropriate for small-scale movement.

Piezoelectric actuators gather the specifications that are adequate for testing a microsample, such as a microscale stroke, nanoscale resolution and the fastest response time.

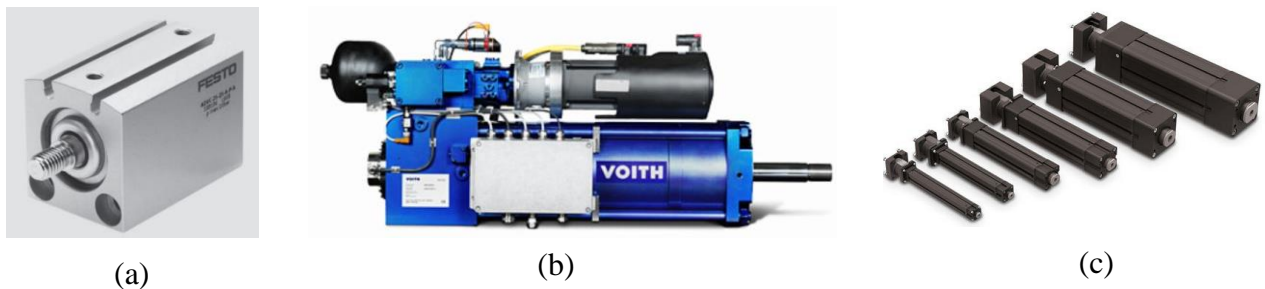


Figure 26 – (a): Festo short stroke actuator [34]; (b) Voith hydraulic actuator system [35]; (c) Tolomatic rod-style linear actuator [36].

3.4.2 Load cell

The load cell available is the MLP-25 of Transducer Techniques. This is a mini low profile load cell for tension or compression with a capacity range of 25 lbs (111.2 N) [20].

This load cell is built with 4 strain gauges mounted in a Wheatstone bridge (Figure 27).

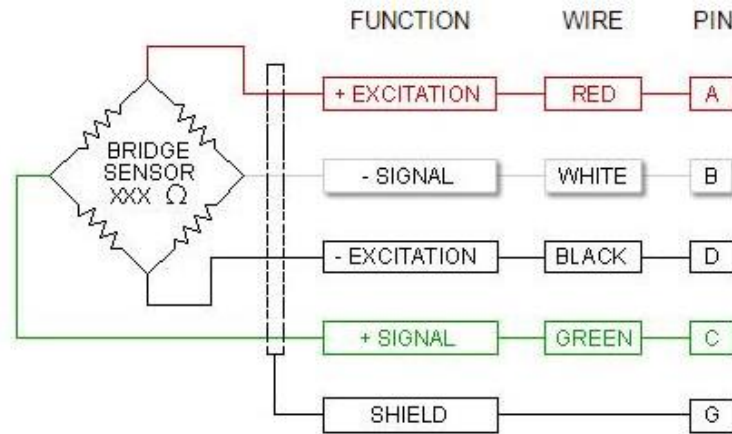


Figure 27 - Wheatstone bridge with load cell wiring [20].

The load cell specifications are the following [20]:

- Capacity range: 25 lbf/111.2 N;
- Rated Output (R.O.): 2mV/V nominal;
- Nonlinearity: 0.1% of R.O.;
- Hysteresis: 0.1% of R.O.;
- Excitation voltage: 10V DC;
- Deflection (at 111.2 N): 76.2 μ m;

The load cell is connected to a DPM-3 load cell meter (Figure 28), this instrument provides the excitation voltage that the load cell needs and read the signal coming from the load cell. Also, it allows connecting easily to the I/O board, through a 0-10V analogic output.



Figure 28 - DPM-3 Digital Panel Mount Load Cell Meter [20].

3.4.3 I/O board

The National Instruments USB-6211 (Figure 29) is the I/O device used in this project. It has 16 analog inputs (16-Bit, 250 kS/s), 2 analog outputs (250 kS/s), 4 digital inputs and 4 digital outputs.

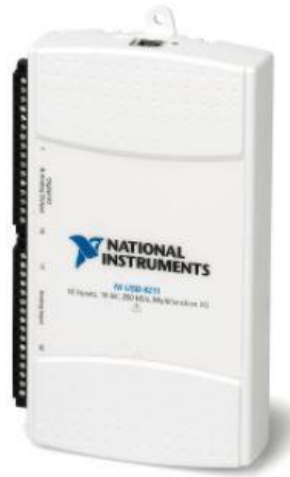


Figure 29 - National Instruments USB-6211 I/O device [37].

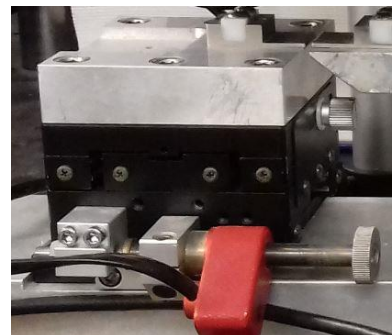
This type of device allows an easy USB connection and therefore control the system using a computer and LabVIEW.

3.4.4 Extra equipment

In order to help with the sample mounting and aligning, the system is equipped with a stage controlled by a picomotor (Figure 30a), this allows small linear displacement.



(a)



(b)

Figure 30 - (a) Newport picomotor [38]; (b) Linear stage.

To allow friction free movement of the structure connected to the piezo actuator an air bearing (Figure 31) was incorporated in the system.

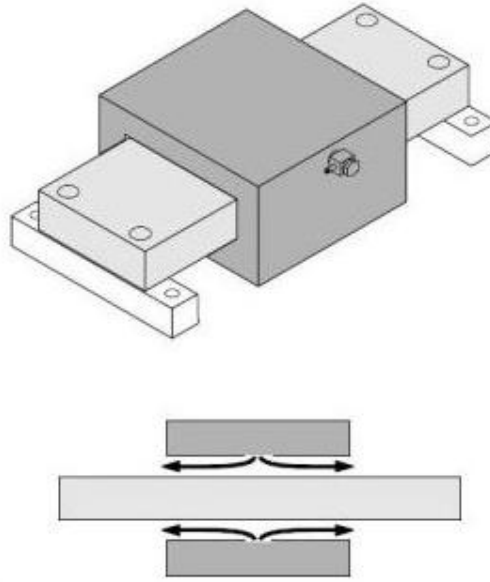


Figure 31 - Air bearing (Top: ISO view; Bottom: Cross section) [39].

Compressed air allows the inner metal bar to float, reducing to friction near to zero.

Comparing to a mechanical bearing means that “there is minimal vibration, hysteresis or reversal error, making it highly repeatable (...). Stiction is virtually eliminated, improving resolution capabilities (...).” [18]. More importantly “Air bearings are virtually frictionless, which means when they are coupled with a direct drive motor or voice coil, they are ideal for micro- and nano-Newton force control applications.” [18], in the particular case of this project means that there is no influence whatsoever of friction inertia, and being this a small scale testing system, having a resistance from a mechanical bearing could compromise the system.

4 Fatigue system

4.1 Introduction

This chapter is dedicated to the developed solution, focusing on the machine itself and the LabVIEW program that controls it as well.

4.2 Physical system

As explained in Chapter 3.4, the machine part of the system is comprised of the piezoelectric actuator, load cell, picomotor, and grips.

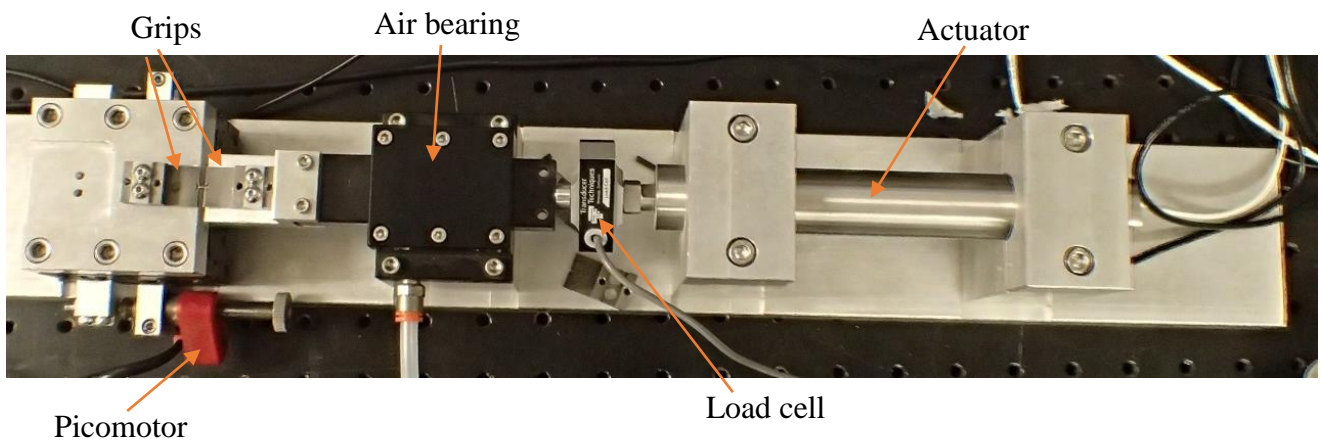


Figure 32 - Fatigue testing system (top view).

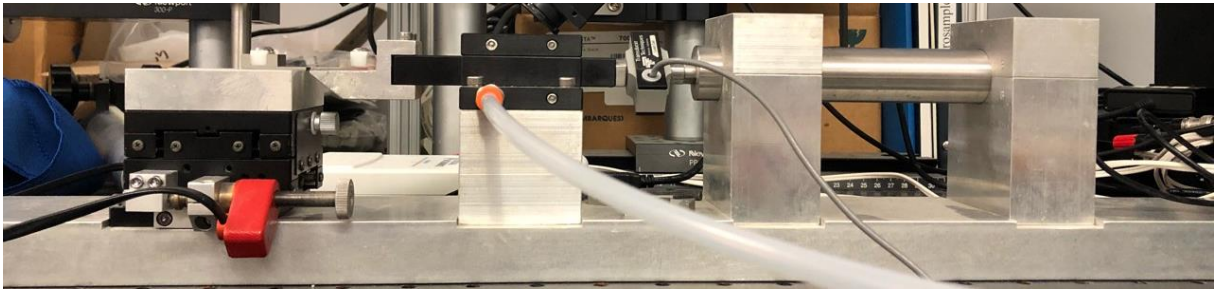


Figure 33 - Fatigue testing system (side view).

Few considerations regarding the relative position of each element:

- The system is placed horizontally (most common assembly is vertical) to allow easy manipulation of the samples;
- Mounting a sample on a horizontal system only requires for it to be dropped in place whilst in a vertical system it is a difficult process of holding the sample in place and placing the grips;
- The order of how each element is placed is somewhat natural, having one grip fixed (during the test this end is fixed but can be moved with the picomotor to help mount the sample) and the other end to be the one that moves. Placing the load cell between the piezoelectric actuator translates in only the moving grip structure to be cantilever;
- With this setup the force transmitted by the piezoelectric actuator is the same value that reaches the sample, therefore the force read by the load cell is the one being applied to the sample;

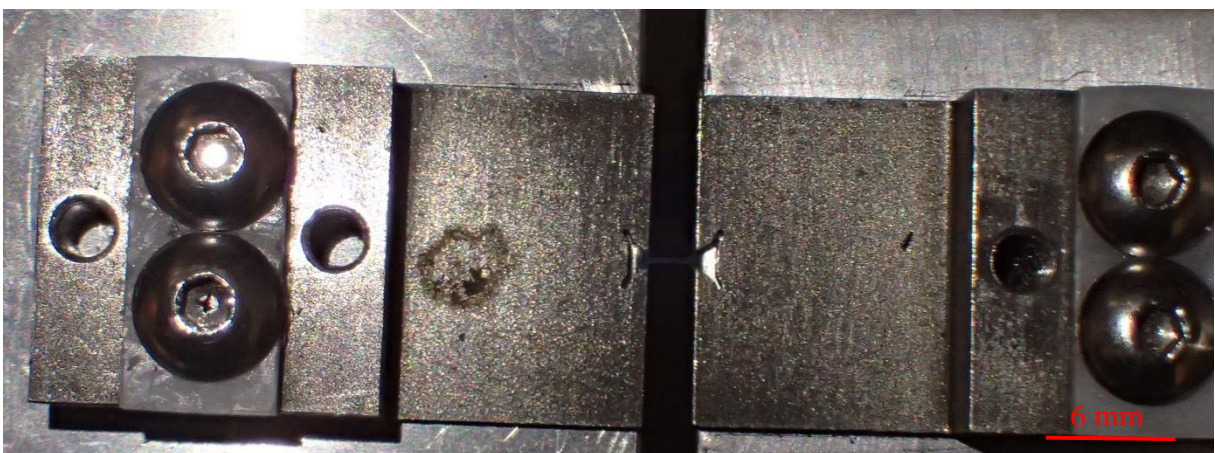


Figure 34 - Grips with sample (top view).



Figure 35 - Grips with sample (lateral view).

4.3 LabVIEW program

The control program is made of three events: resetting the piezo actuator to the zero position, preload stage control, and test phase control. These three structures work independently from each other and only one is active at each time

4.3.1 Piezoelectric actuator reset (first event)

This event moves the piezoelectric actuator to the zero position (zero position is when the actuator is fully extended). The process of this block is if the button “Reset Piezo” is false nothing happens if the same button is true, a Data Acquisition Assistant Express VI is activated. This VI sends the desired output (in this case 10 V) to the I/O board. The voltage out of the I/O board is then connected to the E-508.00 piezo amplifier module that fully extends the piezoelectric actuator. The button has a mechanical action of “latch when released”, which means, after being pressed (true value) it returns to false.

4.3.2 Preload stage (second event)

This structure (Figure 36) loads the sample up to the minimum stress value selected by the user. The base of this block is to successively increment the displacement of the piezo actuator until the minimum stress value is reached.

To achieve this, a while loop creates an integral controller mechanism (repeats itself until the stop condition is reached), increasing the output voltage by 0.01 V in each iteration and checking if the voltage coming in from the load cell is equal to the voltage value of the minimum stress. This conversion is achieved by the load cell properties that can be represented in equation 4.1.

The block labeled as “Write to measurement File2” is used to save the position of the piezoelectric actuator to the next event. This stage is activated by the button labeled “Preload” and does not activate while either the preload or the test stage is running.

$$V = \frac{\sigma \times A}{11.12} \quad (4.1)$$

Where:

V, is voltage in Volts

σ , is stress in Pa

A, is sample cross-sectional area in m²

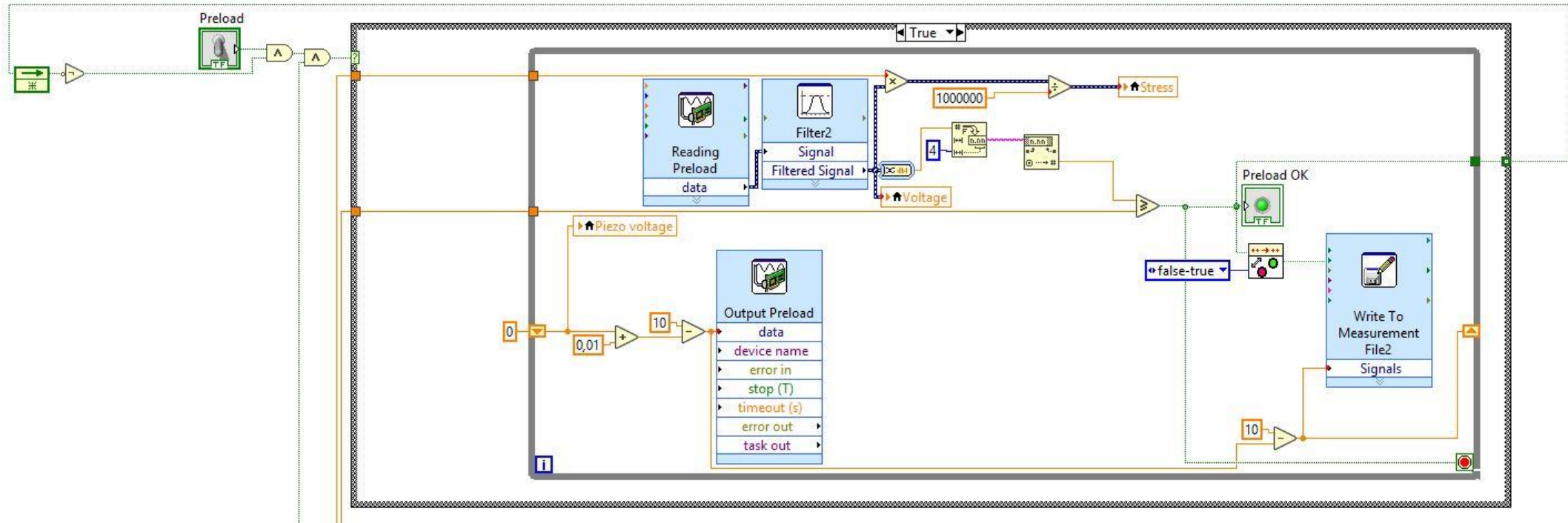


Figure 36 - Preload stage.

4.3.3 Test stage (third event)

This structure is (Figure 39 and Figure 40) controls the test stage and follows the same logic behind the preload stage of successively iterate to reach the desired stress value. It is activated by a button in the front panel once the preload stage is complete.

In Figure 39 starting from the left, the block labeled “Read From Measurement File” gives the position where the preload stage ended and uses this as a starting point of the piezoelectric actuator for the test stage. Above, there is a group of blocks for serial communication with the DIC program (this will be explained later in this section).

Continuing to the right, the block labeled “Reading” reads the voltage outputted by the load cell, this is done continuously so it requires defining a sampling frequency and buffer size. Then the voltage is converted into force by using equation 4.2. This equation was obtained using the data of the load cell and the DPM-3 box and then converted to stress dividing it by the cross-sectional area of the sample inputted by the user.

To the right, there is a subVI, that selects either to increase or decrease load. This subVI is very important and therefore explained in section 4.3.4 Increase/decrease load subVI.

Now in Figure 40, on the left, it is the mathematical operation of increasing or decreasing the output voltage, by 0.0045 V/loop. Also, it is here that if the user selects to run DIC mode, the speed is reduced by changing the increment value to 0.0005 V/loop.

Next is a subVI that counts the number of cycles and checks if the maximum number of cycles, inputted by the user, was reached. This block is shown in Figure 37.

The block “Output” outputs the voltage calculated previously, to the piezoelectric actuator.

To the right, two write to measurement file blocks creates two files with cycle numbers, timestamps and stress values above the maximum stress value and below the minimum stress value. At the end is the structure that sends an e-mail when the test is over (either due to sample failure, stress value overload, or user selection) with the files created attached.

Regarding the DIC, the program runs on another computer and requires a slow displacement and the cycle count (in order to identify which cycle corresponds each picture). To achieve the slow displacement, it was mentioned previously, that once the user switches the DIC button the increment is changed to 0.0005 V/loop until the button is switched off. To transmit the cycle count, TCP/IP communication was tested but the requirement of turning on

the DIC whenever the user pleases it is not compatible with the need to establish connection starting both programs at the same time, characteristic of the TCP/IP communication.

The solution was to switch to serial communication. To establish serial communication, LabVIEW offers a pallet of easy to use blocks, requiring an open communication, a write or read depending if it's on the fatigue testing program or the DIC program, and a close communication block. The port, baud rate, and parity can be hardcoded (Figure 39), only requiring the parity and baud rate to be the same on both programs. This solution requires a serial cable RS-232 null modem and two adapters to USB port because newer computers don't have serial ports.

On the DIC LabVIEW program, the code in Figure 38 is added to receive the data sent by the fatigue testing system through serial communication. This code is similar to the serial communication write used on the test stage structure, but with a few details. The property node "bytes at port" reads how many bytes are being received and sets this number to the reading block (this is very important otherwise it's impossible to read the data).

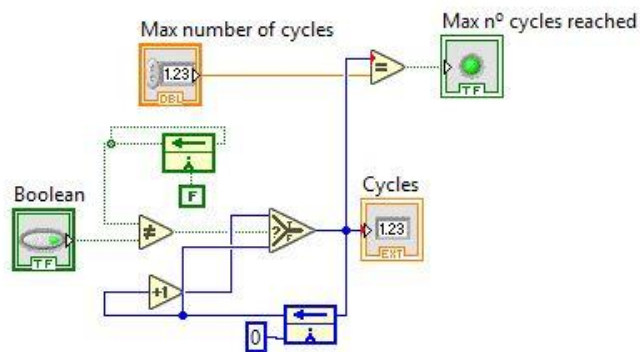


Figure 37 - Max cycles subVI.

$$F = \frac{111,2}{10} \times V \quad (4.2)$$

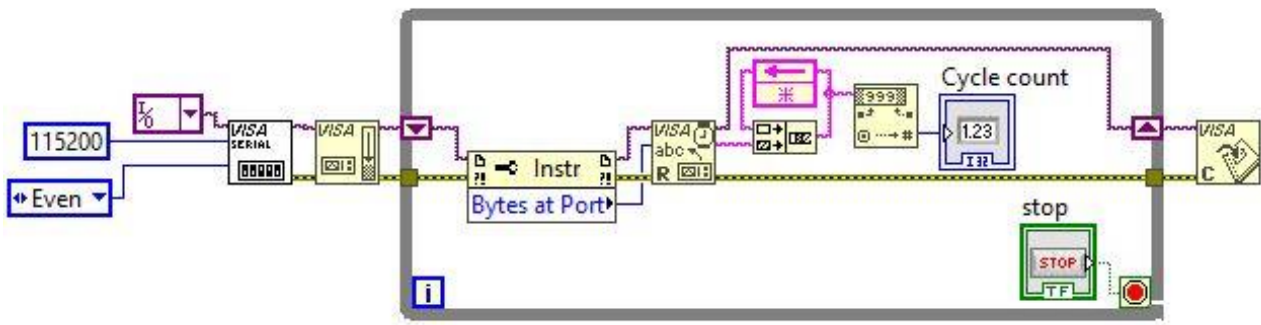


Figure 38 - Serial communication read code.

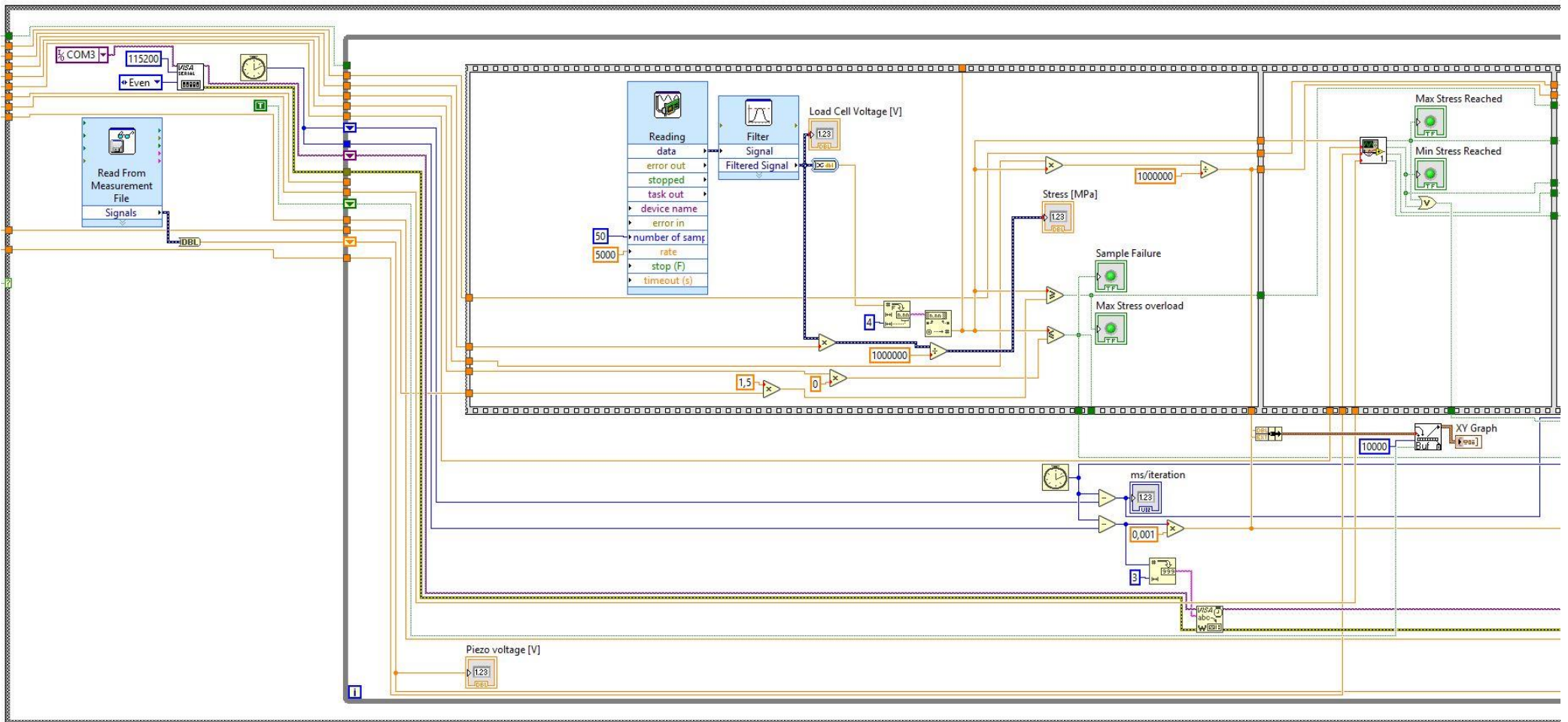


Figure 39 - Test stage.

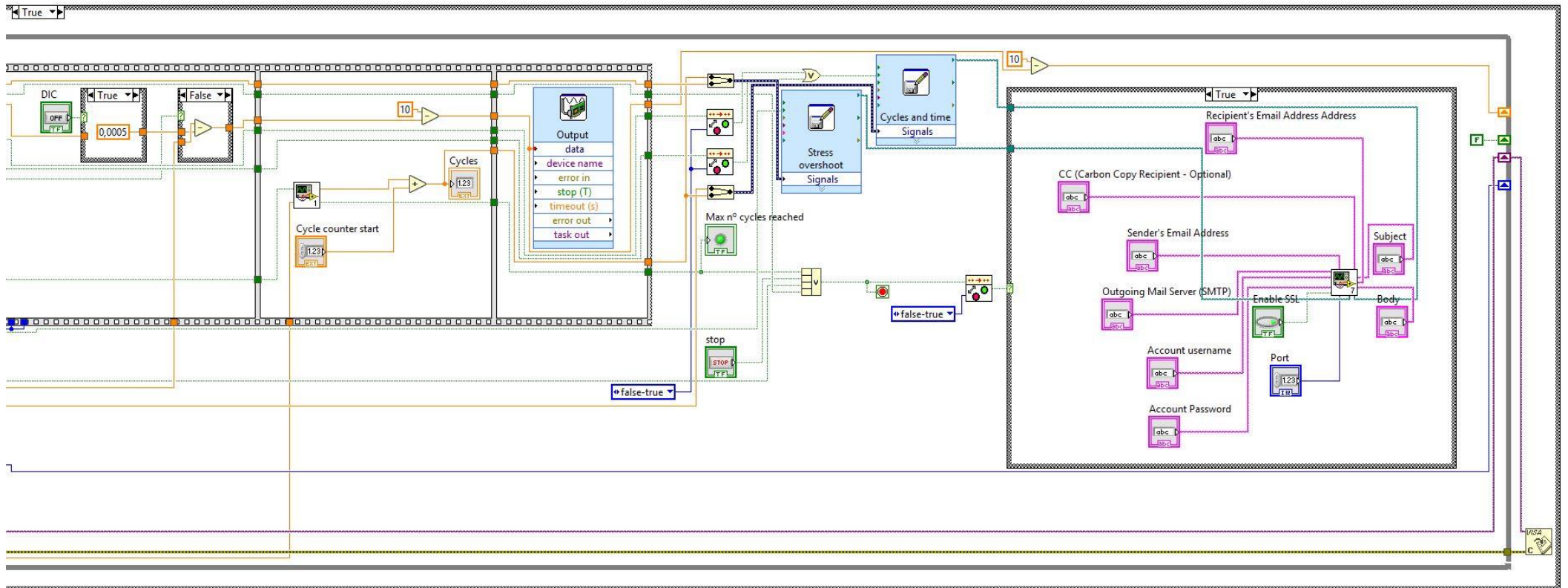


Figure 40 - Test stage.

4.3.4 Increase/decrease load subVI

This program (Figure 41) compares the value of the stress coming from the load cell with the maximum and minimum stress values inputted by the user. Once the stress value reaches either limit a correspondent Boolean variable switch from false to true and changes from increment/decrement to decrement/increment by changing the Boolean variable on the test stage structure.

While testing the program, it was noted that an error occurred. Even though the program detected that the stress value was above or below the maximum and minimum stress value, it would overshoot the value. This happens due to the load cell deflection. Therefore, it was needed to correct this error, this is achieved by “tricking” the program into thinking that the stress value read is actually a corrected value.

Regarding the load cell deflection, it is easy to calculate what the correction factor is, due to the value of the deflection given on the load cell data. The value for the deflection is 76.2 μm , and as shown in Appendix A: Load cell deflection, the correction factor is 0.004.

Regarding other factors that come into play (such as LabVIEW code not being optimized) it is harder to determinate the correction factor. It was noted, during testing, that the overshoot is a function of increment, limit stress values, sampling frequency and buffer size (this is explained in section 5 Results and Discussion). Therefore, through many trials and after finding a stable relation between increment, sampling frequency, and buffer size, the SubVI shown in Figure 41 was achieved.

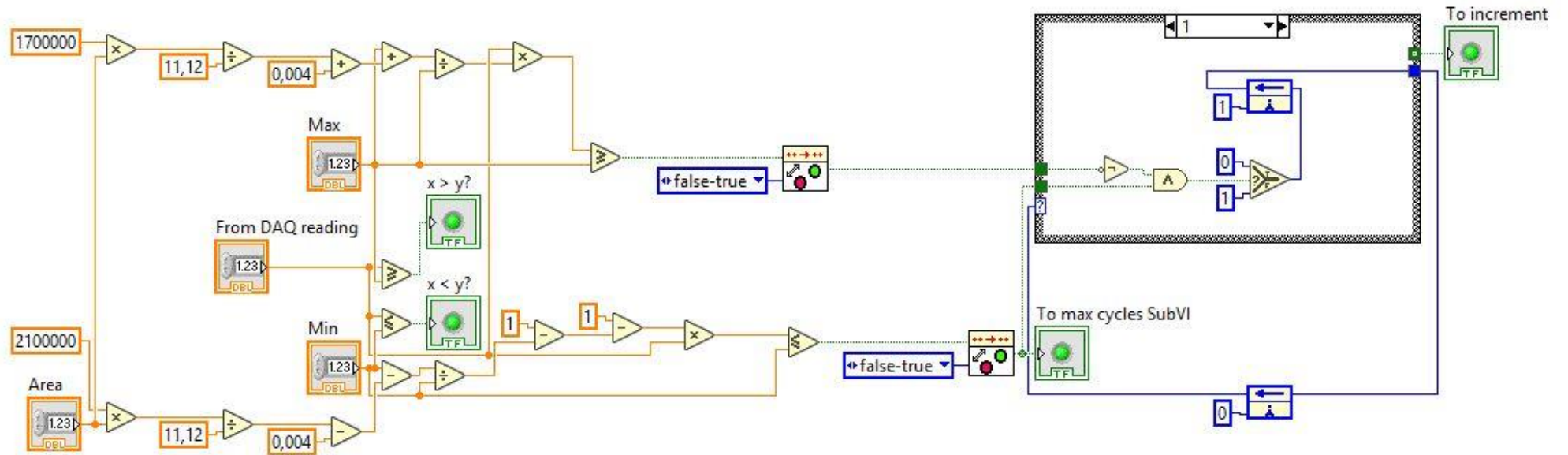


Figure 41 - Increase/decrease load subVI.

4.3.5 Control panel

The control panel (Figure 42) is divided into two sections (left and right), on the left is the e-mail setup section. Here, if the user chooses to, it is possible to configure an e-mail alert once the testing is finished. Depending on the service provider, the user inputs the e-mail server, port and SSL certificate. Afterwards, the e-mail personal information, e-mail subject and message are inserted. Automatically are attached the two files with the test data (one with cycle number and time and the other with cycle number and stress overshoot). It was noted that Outlook service is the one that works the best.


On the right is the test control section. Here is where the user inputs every test parameter, it is also possible to input a number to start counting cycles from it. This allows to stop a test and restart at a different time.

Underneath the input values are the control buttons. The “Reset Piezo” button moves the piezoelectric actuator to its fully extended position. The “Preload” button activates the preload stage and once the “Preload OK” light is on, the “Start Test” button activates the test stage. The “DIC” button turns on/off the DIC mode.

Following is a stress-time graph, this is a visual representation of the test. On the right of the graph is a set of displays that gives real-time data to the user. The “Stress [MPa]” shows the value of stress read by the load cell, it is the same value displayed on the graph. The “Piezo Voltage [V]” allows the user to see how much voltage is being outputted to the actuator, this value should be 0-10 V. The “Load Cell Voltage [V]” permits the user to see if there is an unusual level of voltage coming from the load cell. The max/min stress lights are indicators that show if the stress value is above/below the maximum/minimum stress limits.

At the bottom are the “Sample Failure” and “Max Stress Overload”, the first one indicates that the sample broke, the second one is precautionary of a stress value greater than 50% of the maximum stress limit. This safety feature was incorporated to prevent sample failure due to an unpredictable error.

And finally, the “Stop Test” button.



CROSS SECTION AREA [m²] MAX NUMBER OF CYCLES MIN STRESS [MPa] MAX STRESS

CYCLE COUNTER START CYCLES MAX Nº CYCLES REACHED

MICROSAMPLE FATIGUE TESTING SYSTEM V1.0

OUTGOING MAIL SERVER (SMTP) PORT Enable SSL

ACCOUNT USERNAME ACCOUNT PASSWORD

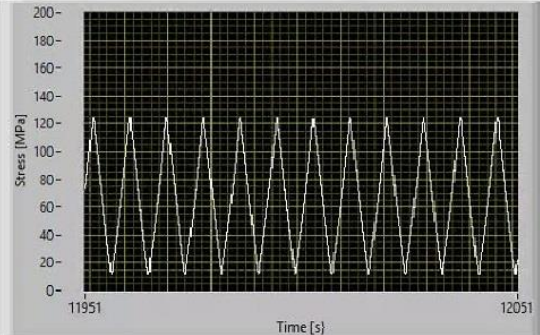
SENDER'S EMAIL ADDRESS RECIPIENT'S EMAIL ADDRESS

CC (CARBON COPY RECIPIENT - OPTIONAL)

SUBJECT

BODY

REST PIEZO PRELOAD PRELOAD OK START TEST DIC



Stress [MPa] vs Time [s]

STRESS [MPa]

PIEZO VOLTAGE [V]

LOAD CELL VOLTAGE [V]

MAX STRESS REACHED MIN STRESS REACHED

ms/ITERATION

SAMPLE FAILURE MAX STRESS OVERLOAD

Figure 42 - Control panel.

4.3.6 Fatigue testing (alternating stress amplitude)

One extra goal of this dissertation was to provide one separate program that could provide the ability to perform fatigue testing with alternating limits of stress. This means, performing a set of cycles at one pair of maximum and minimum stress limits and then performing another set of the same number of cycles but with a different pair of maximum and minimum stress limits. The interest in this type of testing comes from the real world where a part is never subjected to the same load amplitude.

Based on the original fatigue testing program, a few modifications were required to achieve the type of testing desired.

The test stage structure is the one that had to be altered, while every other structure remained the same.

A subVI (Figure 43) divides the current number of cycles by the block size that was inputted by the user. Every time the remainder is equal to zero, which means a number of cycles equal to the block size have passed, a Boolean variable switch from false to true and as a consequence selects, on the main VI, the pair of stress limits that was not activated on the previous set of cycles.

Regarding the user interface, it is similar to the Figure 42, with the added inputs for block size and the 4 stress limits.

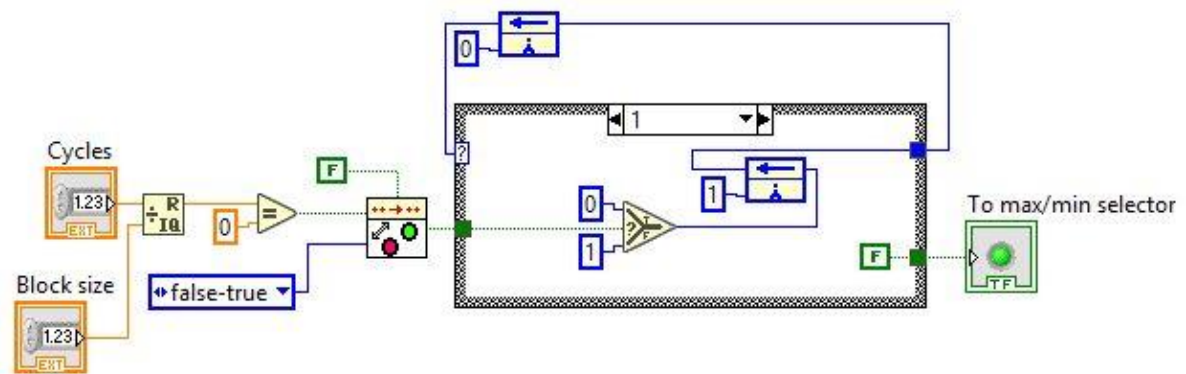


Figure 43 - Block counter subVI.

5 Results and Discussion

This project was developed to increase the mechanical characterization ability at the Micro Materials Characterization lab and as a result take a step forward at better understanding AM technology.

The main goal of this dissertation is to have a system capable of performing standard fatigue testing on a micro sample. To achieve a fatigue system an open loop architecture was required, where the load is applied to a sample and a sensor gives feedback information to the controller. There are many ways to achieve this, some more expensive and complex, others are simpler and cheaper. The approach taken was to choose simple and with room for improvement. With the mechanical system composed of a piezoelectric actuator, a load cell, an air bearing, sample holder and a linear stage. Assembling the system, the way that it's shown in Figure 32, guarantees that the load cell and actuator are not cantilever, therefore do not affect the sample.

The basic logic behind the controller program is to repeat an operation to increase the load applied to the sample until the maximum stress limit is reached, then to decrease the load applied until the minimum stress limit is reached, repeat until the stop conditions are achieved. This logic automatically relates to a while loop in LabVIEW language. To obtain the stress value in real-time, data is obtained from the load cell (voltage), therefore data acquisition through an I/O board is the best option, through the use of the integrated software and hardware from National Instruments. At the same time, to apply the load on the sample, using a piezoelectric actuator that requires a 0-10 V input, the solution is again using LabVIEW and an I/O board.

The data acquisition resolution is given by the analogic to digital conversion. With device range of ± 5 V this means a maximum of 55.6 N and as a result, 889 MPa which is more than enough for the materials that are tested. With this range chosen (granted that it can be changed at any time), the precision of the data acquisition of the 16-bit NI USB-6211 is 152.6 μ V.

Still related to the data acquisition is the overshoot error. The way the program works, it needs to go over the limit values to switch events, this is to prevent errors like hysteresis, any undesired movement, and any other unpredictable errors. When the sampling frequency and buffer size are set to very high numbers (slow execution speed) the overshoot is close to zero. Using the relation mentioned previously, an unacceptable overshoot appears that needs to be corrected. The way to do it is explained in section 4.3.4 Increase/decrease load subVI. Due to the overshoot being a function of the stress limits it would require many iterations until a correction factor that works for any stress amplitude to be found. During testing to overcome this error it was noted that if a big correction was made on a cycle with high maximum stress (e.g. 186 MPa) when a low maximum stress (e.g. 100 MPa) cycle was being tested it wouldn't reach the limit values, and therefore data would be lost. So, it was decided to have a bigger overshoot (around 1 MPa) on cycles with high-stress amplitude to allow on cycles with less stress amplitude to run without errors and having a 1 MPa overshoot on a high-stress amplitude and high maximum stress limit is not significant. Traditionally, in other positioning systems, a PID controller is able to reduce overshoot but, in the case of this system, the intention is not to move the actuator between two defined positions, is to increase load successively and check if the desired value was reached. Also, a PID controller introduces a slope when approaching the goal, and in fatigue testing is important to have constant displacement over time.

Regarding the user interface, it was tried to keep it as simple and pragmatic as possible, in order to not confuse the user independently if it is familiar with the system or not. Therefore, the control panel is organized into two halves, the left setups the e-mail alert and the right are the test controls. Labels help to understand how to use the program and a user's manual was written (Appendix B: User's manual).

The ultimate goal of this project was to build a system capable of applying cyclic load between two stress values through time until the end condition is reached. That goal was achieved as shown in Figure 44, taken from a test of an AlSi10mg sample made by DMLS and tested at 90% yield ($\sigma_{\max}=186$ MPa).

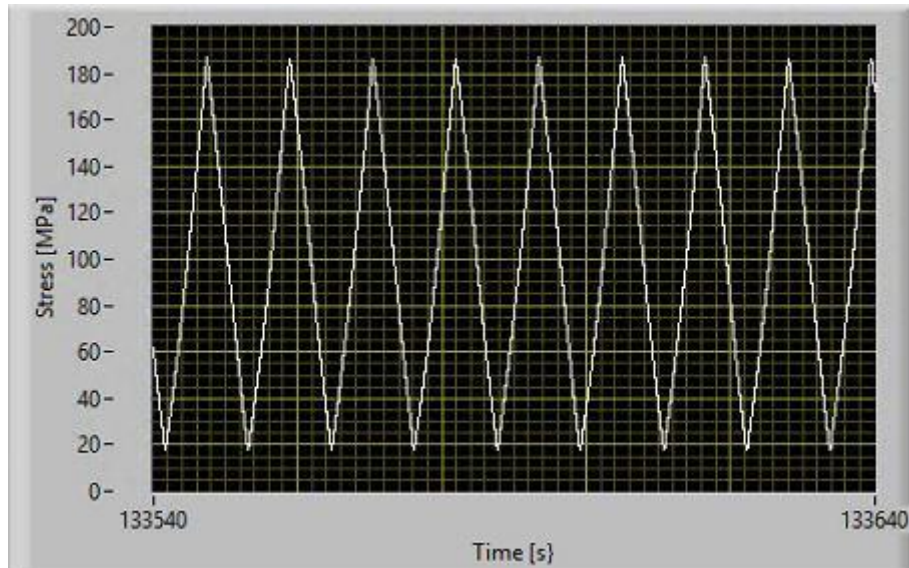


Figure 44 - Stress/time graph fatigue testing.

The program itself can run without errors but that doesn't mean full test runs without any error. Due to the system being operated on a computer that runs on Windows 10 operating system (and not on a closed system like a commercial machine) some errors might appear. With the program running for an extended period, is possible for the computer to lose "focus" on the program and start doing background tasks, switching processing memory to other operations and as a result, a buffer size error might appear. Some measures to prevent this can be taken, such as increasing the LabVIEW priority on the task manager (if it's set to real-time the computer will allocate all of its power to LabVIEW), clear memory by rebooting the computer before starting a test. Even if an error of this kind occurs, it is always possible to restart the test at the cycle number it stopped, due to the nature of fatigue, the fatigue life is cumulative meaning it doesn't matter if the test is stopped and restarted as long as the limit stress values are the same.

As for the alternating amplitude request, it required the inclusion of a subVI to perform sets of cycles alternating between the two pairs of stress limits defined by the user, as seen in Figure 45, a block of three cycles performs with each set of stress limits.

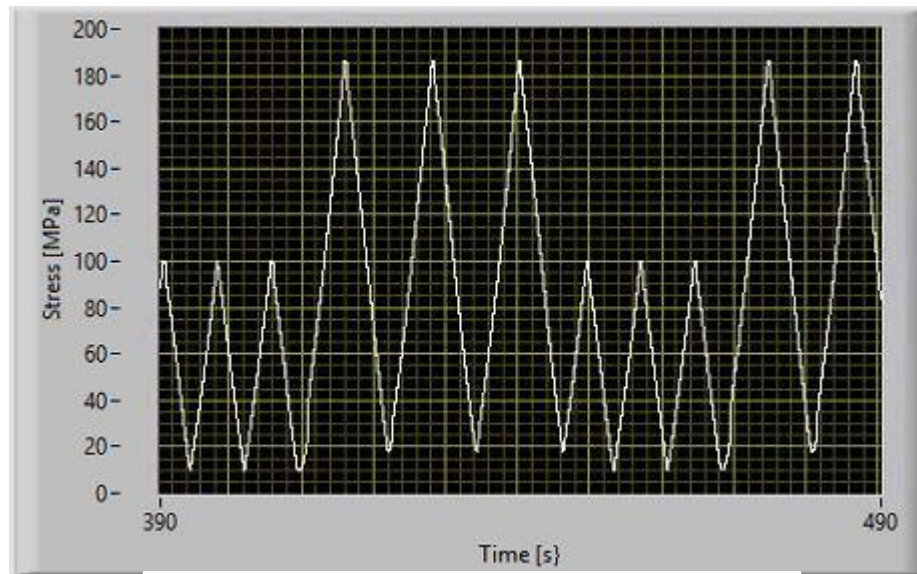


Figure 45 - Stress-time graph of alternating stress amplitude.

During testing, it was noted that the linear stage was not completely immobile, though it is not enough to affect test results (it requires a bit more displacement by the actuator) it is something to be corrected in the future.

Regarding the DIC system, a specialized camera and objective (Figure 11) were installed on the fatigue testing system. The system operates from another computer and it requires communication between both LabVIEW programs. The first idea to solve this problem was using TCP/IP protocol through ethernet but it did not work. It required communication between the fatigue testing program and DIC program to be established as soon as the fatigue program was started, making it impossible to utilize LabVIEW on the DIC computer while fatigue testing hasn't finished, which can take days). Serial communication using RS-232 null modem cable solved this problem. Communication can be established and terminated at any time responding to user needs. Using DIC requires the test frequency to be around 1 min per cycle, and that is easily achieved by switching the loop increment.

5.1 Fatigue testing results

Once this system was proved to work and to be reliable, it was time to start fatigue testing. Several samples of AlSi10mg were prepared, from different directions (x,y,z) and tested at multiple stress values, shown in Table 4.

Table 4 - Fatigue testing results.

Direction	Yield strength [MPa]	Min Stress [MPa]	Max Stress [MPa]	Cycles
Z (surface)	Unknown	10	100	13000
Z ₃₄ (core)	207	18.6	186	107109
Z ₃₅ (core)	207	16.5	165	131194
Z ₃₃ (core)	207	12.4	124	177289 ⁽¹⁾

The tests were performed with no major issue, the stress limits were maintained at an acceptable level with no unusual peak values. Frequent test control was performed to ensure the stability of the program.

The samples from core material perform in a “traditional way” following a Wohler’s curve, even if at a lower fatigue life when compared to an aluminum of identical yield strength ([21]), which is expected from an AM part. And as shown in Figure 46 and Figure 47, it appears that there is no unusual trait, such as voids, and that can help explain the traditional fatigue behaviour. The interesting result is the one from a surface sample, which performed at an unusual bad level (low fatigue life for low-stress amplitude), and as shown in Figure 48, there is a depression on the bottom right corner. Being this defect near the surface of the sample, it is possible that it is responsible for the low fatigue life at such low stress amplitude. Fatigue life is affected by defects and surface roughness, even though the samples were polished before testing, a defect such as the one in this sample, especially when connected to the right side of the sample where it is not possible to polish, and as such the surface roughness is higher, could be the cause of failure.

(1) Test stopped due to time availability.

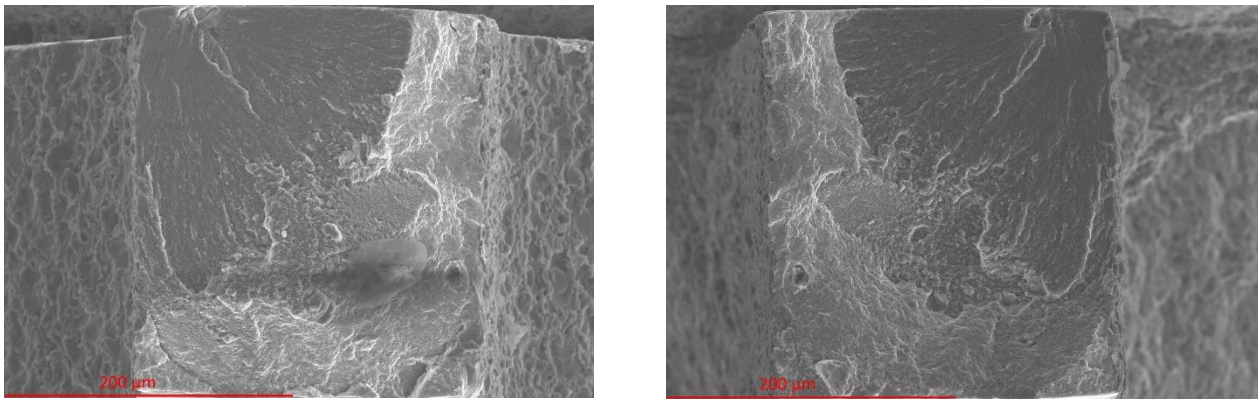


Figure 46 - Z₃₄ (core) fracture 1000x.

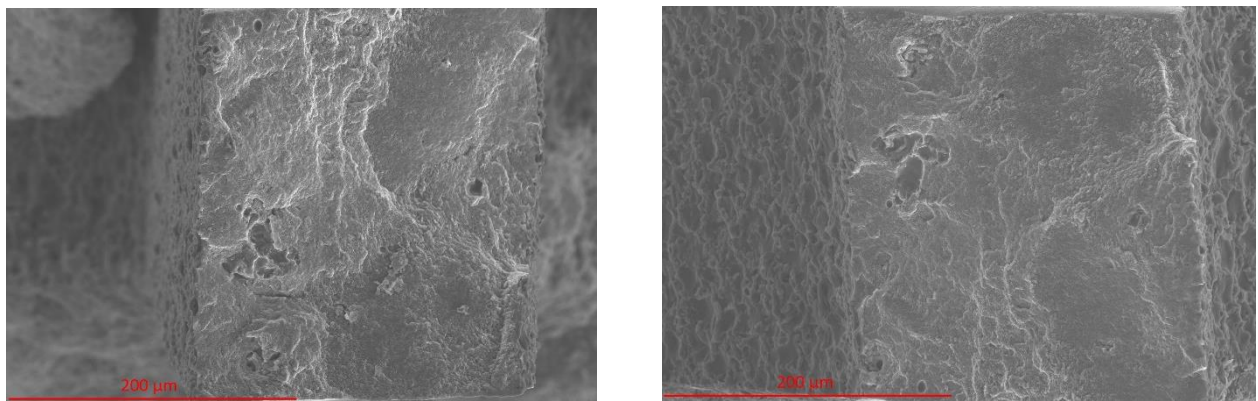


Figure 47 - Z₃₅ (core) fracture 1000x.

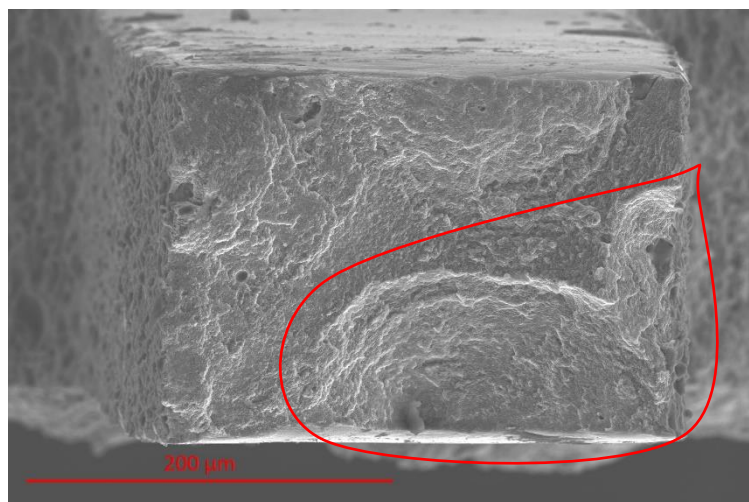


Figure 48 - Z (skin) fracture 1000x.

6 Conclusions

The ultimate goal of this project was to build a system capable of applying cyclic load between two stress values through time until the end condition is reached. That goal was achieved and a simple and reliable system was established. Every requirement was achieved.

The proposed solution is able to perform the type of testing desired with no major problem.

The equipment used to build the machine satisfies the requirements for this type of testing, namely, the piezoelectric actuator is the ideal choice regarding the magnitude of displacement needed. The load cell is sufficient for this application, and the DPM-3 box when unfiltered, constitutes no hindrance to the speed of testing.

The LabVIEW program is enough to perform testing at a prototype level, even with the adjacent problems of running a machine on an open system. National Instruments provides simple and integrated solutions for data acquisition and voltage output, ideal to use on a prototype of this kind.

The total cost of the system is close 10000\$, it is a considerable value but still below any commercial machine price which is not capable of performing microsample testing. With this price tag, it is possible to build multiple systems to run various tests at the same time.

The fatigue tests performed showcase a discrepancy between the fatigue life of surface and core materials. The core materials follow a traditional Wohler's curve whilst the surface material failed at a low cycle count while being tested at a low amplitude. This highlights the need to further investigate the mechanical behavior of AM parts in order to fully understand this technology.

This experience was incredible and unexpected in the course of my academic career. Besides having the opportunity to travel and getting to know a new country, it was above it all, a time of learning not only on the academic (and professional) side but on the personal as well. It allowed me to break my routine at FEUP and leave my comfort zone, providing me a new understanding to define priorities in my professional future and set personal goals.

I had to learn how to live away from home and family, learn how to deal with day by day situations, understand how to connect and speak with people from different cultures and backgrounds, and improve my level of English language.

UMBC is now my home away from home and I hope to have there a place for future projects, allowing me to keep growing not only as an engineer but as a person as well.

6.1 Future development and research

Even though the system performs as it was intended, there is always room for improvement, and some suggestions are summed up next:

- Determine the sampling frequency and buffer size that best fit this application and allows for the fastest loop time;
- Perfect the LabVIEW code, correcting any misusing of elements and trimming it to run smoothly;
- Fit a capacitance gage to the system to measure displacement;
- Improve the linear stage to maintain it locked in the same position during testing;

References

- [1] ASTM International, “F2792-12a - Standard Terminology for Additive Manufacturing Technologies,” 2013.
- [2] J. C. do C. Santos, “A Qualification Methodology for Additively Manufactured Parts University of Maryland , Baltimore County”, Integrated Masters thesis,” FEUP/UMBC, 2016.
- [3] K. V. Wong and A. Hernandez, “A Review of Additive Manufacturing,” *ISRN Mech. Eng.*, vol. 2012, pp. 1–10, 2012.
- [4] W. J. Sames, F. A. List, S. Pannala, R. R. Dehoff, and S. S. Babu, “The metallurgy and processing science of metal additive manufacturing,” *Int. Mater. Rev.*, vol. 61, no. 5, pp. 315–360, Jul. 2016.
- [5] M. Shellabear and O. Nyrhilä, “DMLS – Development History and State of the Art,” *Lane 2004*, pp. 1–12, 2004.
- [6] C. Meier, R. Penny, Y. Zou, J. S. Gibbs, and A. J. Hart, “Thermophysical Phenomena in Metal Additive Manufacturing by Selective Laser Melting : Fundamentals , Modeling , Simulation and Experimentation,” pp. 1–65, 2016.
- [7] W. E. Frazier, “Metal additive manufacturing: A review,” *J. Mater. Eng. Perform.*, vol. 23, no. 6, pp. 1917–1928, 2014.
- [8] J. Coykendall, M. Cotteleer, L. Holdowsky, and M. Mahto, “3D opportunity in Aerospace and Defense,” *Deloitte University Press*, pp. 1–28, 2014.
- [9] B. Stucker and D. Justin, “Improving Implants Using Laser-Based Metal Deposition Technologies,” *Bonezone*, no. Spring, pp. 22–25, 2006.
- [10] W. D. Callister Jr., *Materials Science and Engineering: An Introduction*. John Wiley & Sons, Inc, 2007.
- [11] N. McCormick and J. Lord, “Digital image correlation,” *Mater. Today*, vol. 13, no. 12, pp. 52–54, 2010.
- [12] S. Nimer, J. Wolk, and M. Zupan, “Location and Orientation Specific Material Property Evaluation of Friction Stir Welded Ti-5111: A Microsample Approach,” *Adv. Eng. Mater.*, vol. 16, no. 4, pp. 452–458, Apr. 2014.
- [13] M. Zupan, “Microsample Characterization of the Tensile and Compressive Mechanical Properties of Single Crystalline Gamma-TiAl,” Johns Hopkins University, USA, 2000.
- [14] J. Wolk, “Microstructural Evaluation in Friction Stir Welding of TI 5111,” University of Maryland, College Park, USA, 2011.
- [15] ASTM, “Standard Practice for Conducting Force Controlled Constant Amplitude Axial Fatigue Tests of Metallic Materials,” *Test*, vol. 3, no. Reapproved, pp. 4–8, 2002.
- [16] A. Pineau, “Low-Cycle Fatigue,” in *Fatigue of Materials and Structures*, John Wiley & Sons, Inc., 2013, pp. 113–177.
- [17] T. Nicholas, G. Sendeckyj, O. Davenport, P. Randall, A. Kallmeyer, B. Bartha, T. Farris, J. Calcaterra, J. Zuiker, “High Cycle Fatigue - A Mechanics of Materials Perspective,” Oxford: Elsevier Science Ltd, 2006, pp. 145–212.
- [18] P. Instrumente, “Piezoelectric actuators.” [Online]. Available: <https://www.physikinstrumente.com/en/>. [Accessed: 06-Nov-2017].

- [19] P. Instrumente, “P-239.90.” [Online]. Available: <http://www.pi-usa.us/index.php>. [Accessed: 06-Nov-2017].
- [20] “Transducer Techniques.” [Online]. Available: <https://www.transducertechniques.com/>. [Accessed: 07-Nov-2017].
- [21] H. Ozdes, “The Relationship Between High-Cycle Fatigue and Tensile Properties in Cast Aluminum Alloys,” *UNF Theses and Dissertations*, 2016.
- [22] VPG Transducers, “Technical Note VPGT-02,” 2015.
- [23] D. Ding, Z. Pan, D. Cuiuri, H. Li, and S. van Duin, “Advanced Design for Additive Manufacturing: 3D Slicing and 2D Path Planning,” in *New Trends in 3D Printing*, InTech, 2016, p. Ch. 01.
- [24] “Turbine blade.” [Online]. Available: <https://slm-solutions.com/>. [Accessed: 27-Oct-2017].
- [25] “EOS radiator.” [Online]. Available: <https://www.eos.info/en>. [Accessed: 27-Oct-2017].
- [26] “Tension/tension cycle.” [Online]. Available: <https://www.nde-ed.org/>. [Accessed: 30-Oct-2017].
- [27] “Zwick/Roell HA series.” [Online]. Available: <https://www.zwick.com/>. [Accessed: 31-Oct-2017].
- [28] “Instron E1000.” [Online]. Available: <http://www.instron.us/en-us>. [Accessed: 31-Oct-2017].
- [29] K. K. Alaneme, “Design of a Cantilever -Type Rotating Bending Fatigue Testing Machine,” *J. Miner. Mater. Charact. Eng.*, vol. 10, Jan. 2011.
- [30] Y. Ochi, T. Matsumura, K. Masaki, and S. Yoshida, “High-cycle rotating bending fatigue property in very long-life regime of high-strength steels,” *Fatigue Fract. Eng. Mater. Struct.*, vol. 25, no. 8/9, pp. 823–830, Sep. 2002.
- [31] “Fatigue testing machines.” [Online]. Available: <http://fgg-web.fgg.uni-lj.si/~pmoze/ESDEP/master/wg12/10200.htm>. [Accessed: 02-Dec-2017].
- [32] Y. L. Lee, J. Pan, R. Hathaway, and M. Barkey, *Fatigue Testing and Analysis: Theory and Practice*. Elsevier Science, 2011.
- [33] D. A. LaVan and W. N. Sharpe, “Tensile testing of microsamples,” *Exp. Mech.*, vol. 39, no. 3, pp. 210–216, 1999.
- [34] “Festo.” [Online]. Available: <https://www.festo.com/>. [Accessed: 29-Nov-2017].
- [35] “Voith.” [Online]. Available: <http://voith.com/>. [Accessed: 30-Nov-2017].
- [36] “Tolomatic.” [Online]. Available: <https://www.tolomatic.com/>. [Accessed: 30-Nov-2017].
- [37] “National Instruments.” [Online]. Available: <http://www.ni.com/en-us.html>. [Accessed: 07-Nov-2017].
- [38] “Newport picomotor.” [Online]. Available: <https://www.newport.com/>. [Accessed: 14-Nov-2017].
- [39] “Air bearing.” [Online]. Available: <https://electromate.wordpress.com/tag/air-bearing-linear-tables/>. [Accessed: 14-Nov-2017].

Appendix A: Load cell deflection

In an ideal universe, the load cell would be completely rigid and therefore, would not deform. In reality, this doesn't happen and therefore it is needed to account for this error. The best way to explain is to use a stay rod, see Figure 49.

“Stay rods are used if major load movement is anticipated, for example in weighbridges or vessels with an agitator. Stay rods are installed horizontally and should not transfer any forces (...)” [22].

The vertical component of the force can be calculated through:

$$F_p = F_s \times \frac{d}{l}$$

Where:

F_p , is the vertical component along the principal axis of the load cell

F_s , is the side force

d , is the load cell deflection

l , is the length between the points of contact of the load cell and the system

Applying to the MLP-25 load cell ($d = 0.003$ inch or 0.0762 mm and $l = 0.750$ inch or 1.905 mm):

$$\frac{F_p}{F_s} = 0.004$$

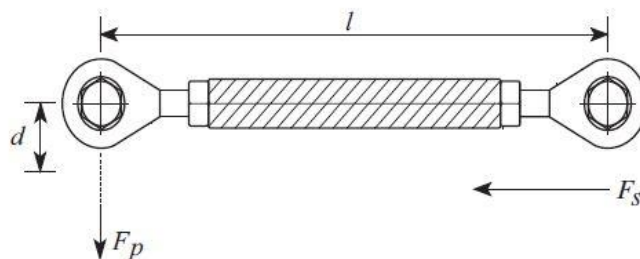
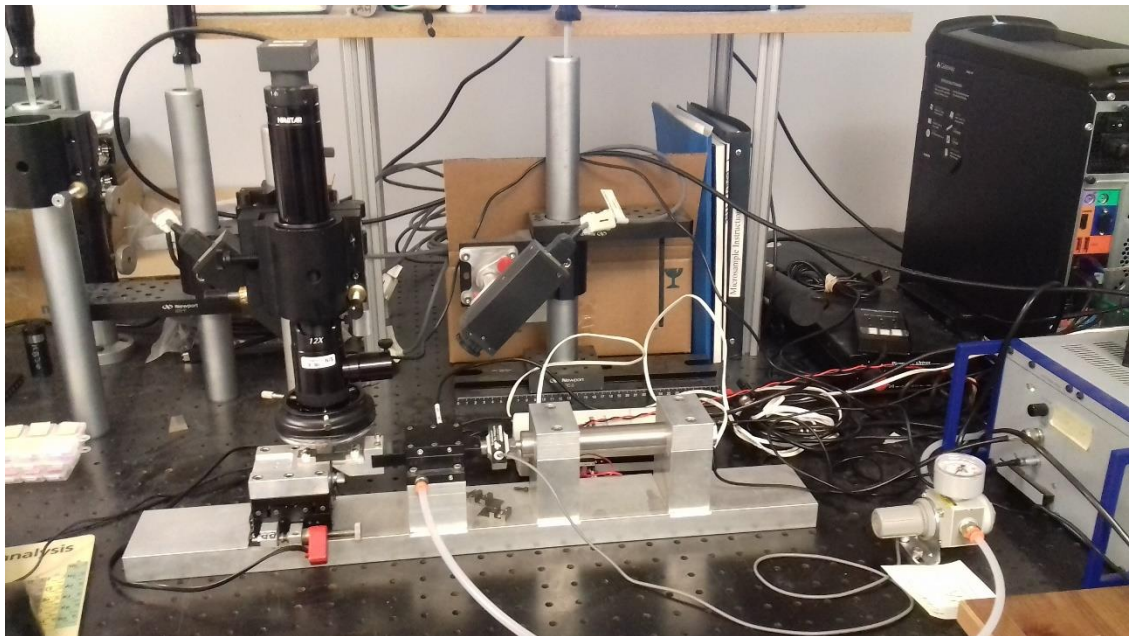
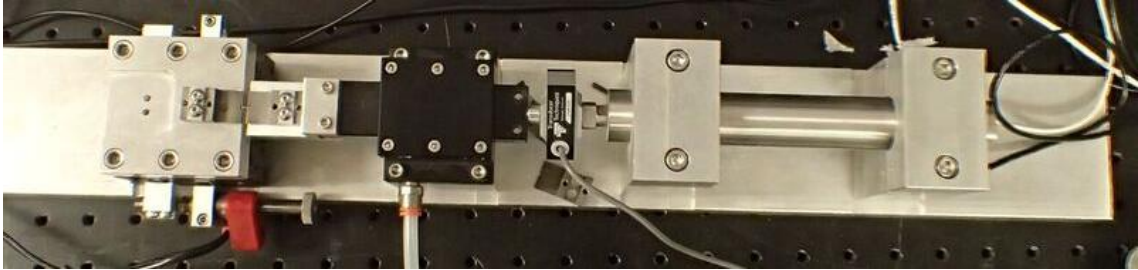


Figure 49 - Stay rod representation [22].

Appendix B: User's manual

System overview:

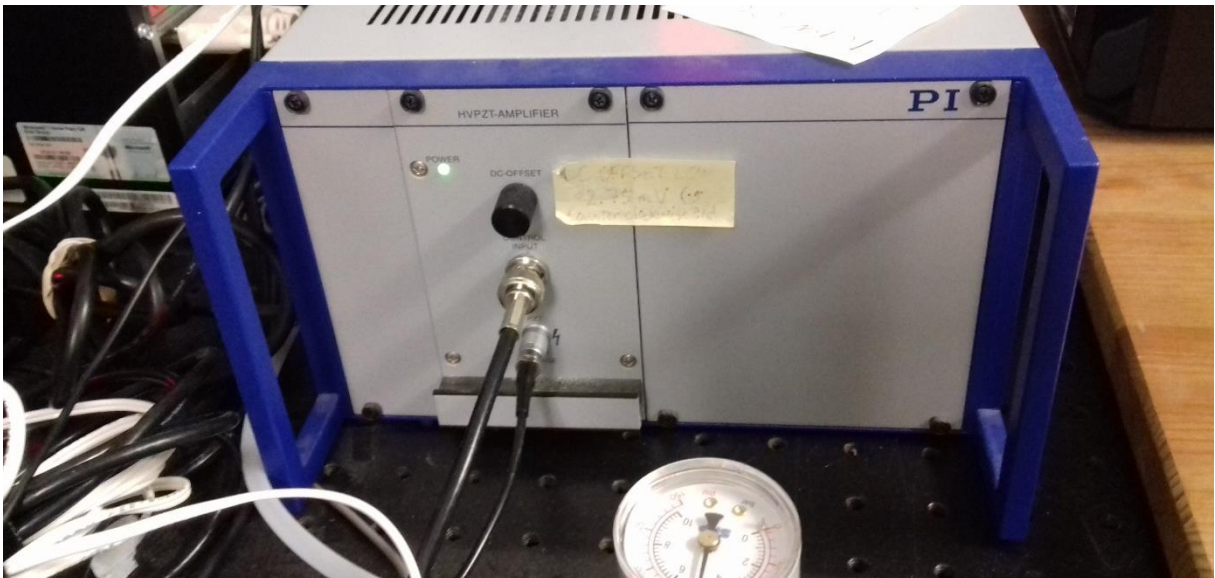


Testing Setup

1. Turn on system;
 - a. Load cell box;

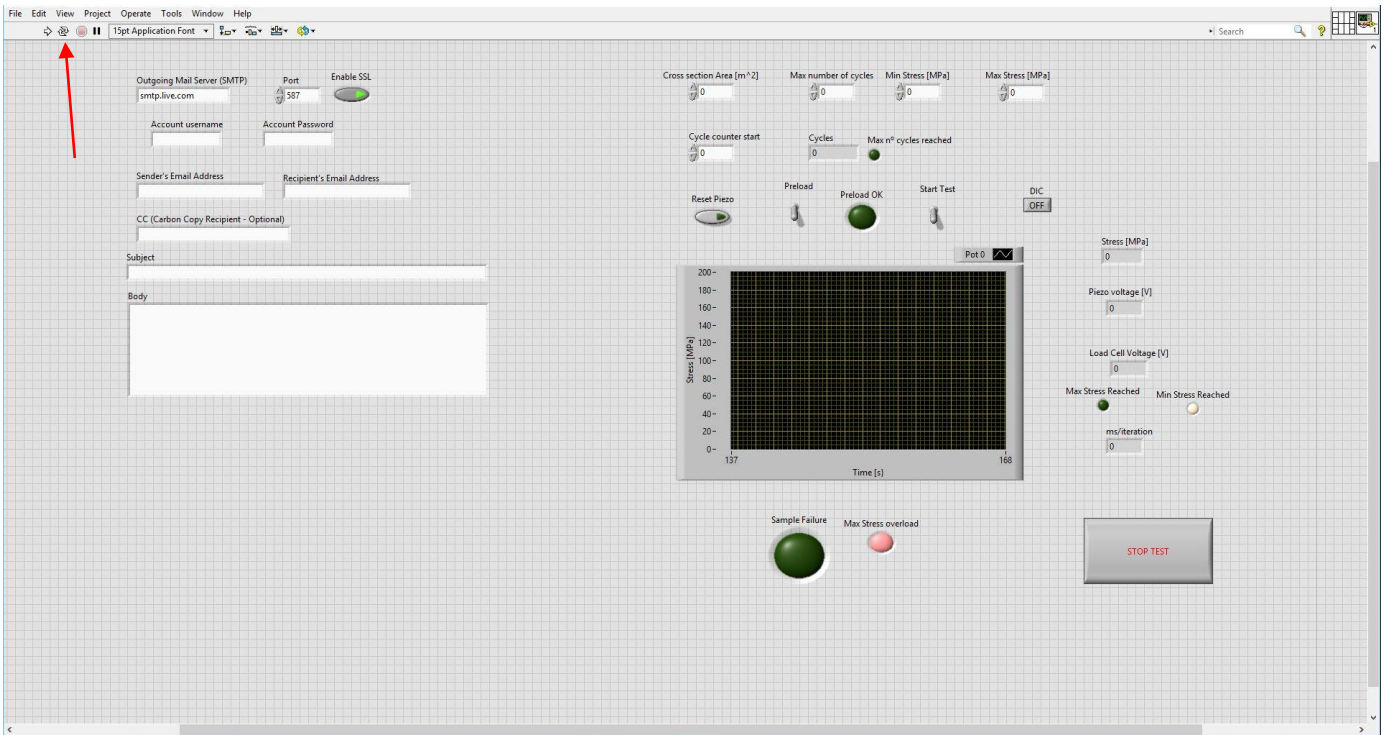


- b. Piezo Controller;

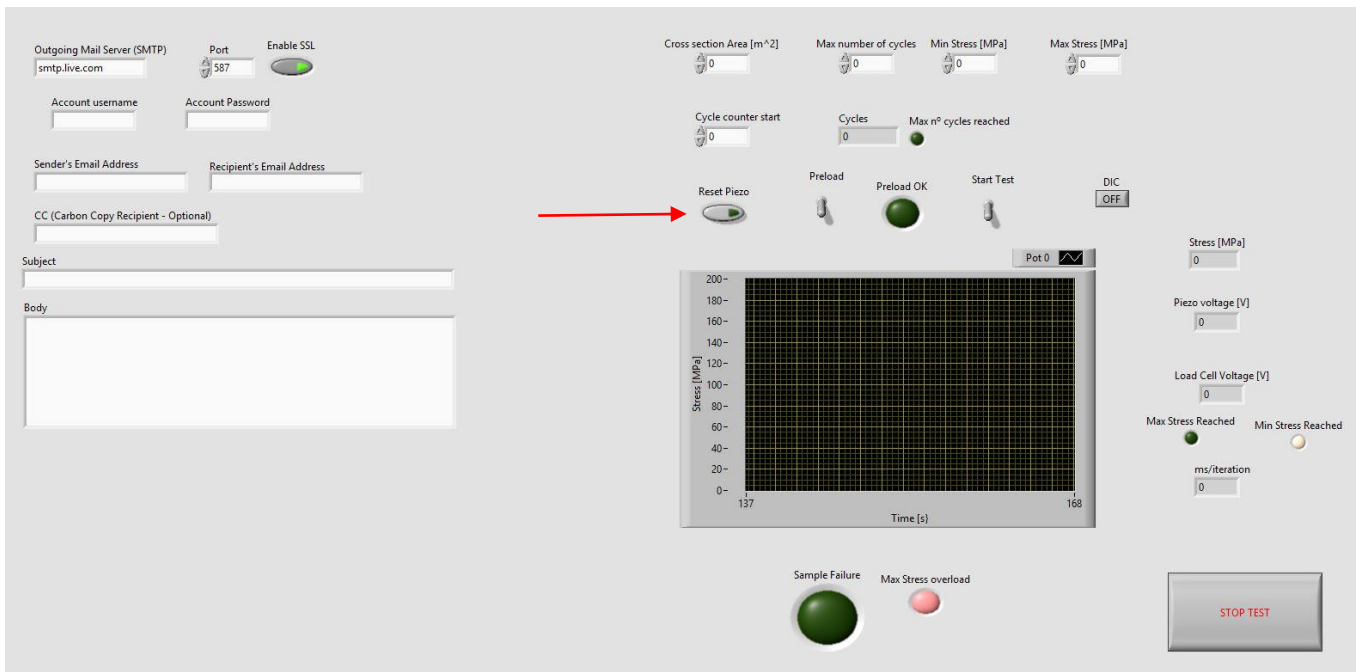


- c. Set air to 50 psi;
 - d. Open LabVIEW;

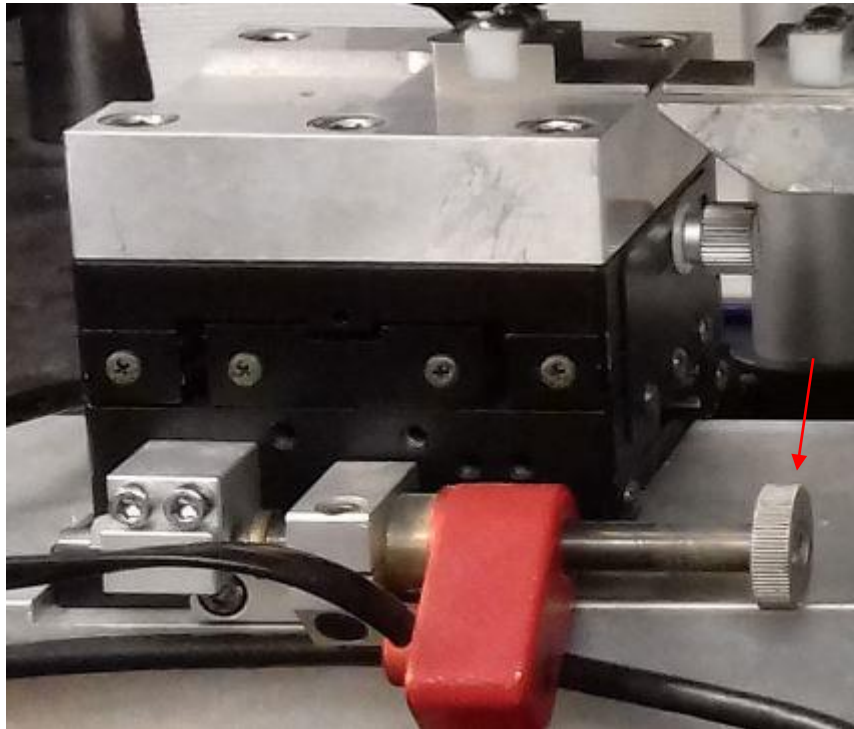
2. Open LabVIEW Program;
 - a. Click run continuously;



- b. Click *RESET PIEZO* button;



3. Adjust picomotor stage using the screw;
 - a. About specimen length;



4. Tare Load cell box;
 - a. Third button from the left;

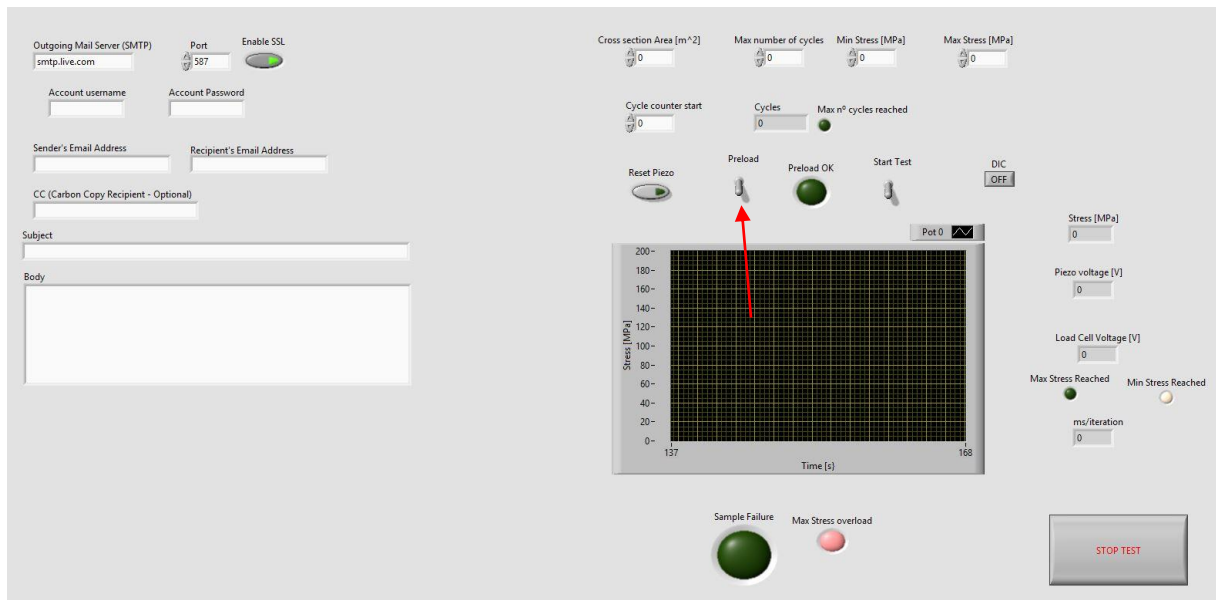


5. Drop sample into grips;
 - a. Adjust picomotor linear stage with the controller until you reach a non-zero value;
 - b. Adjust back to zero on load cell;



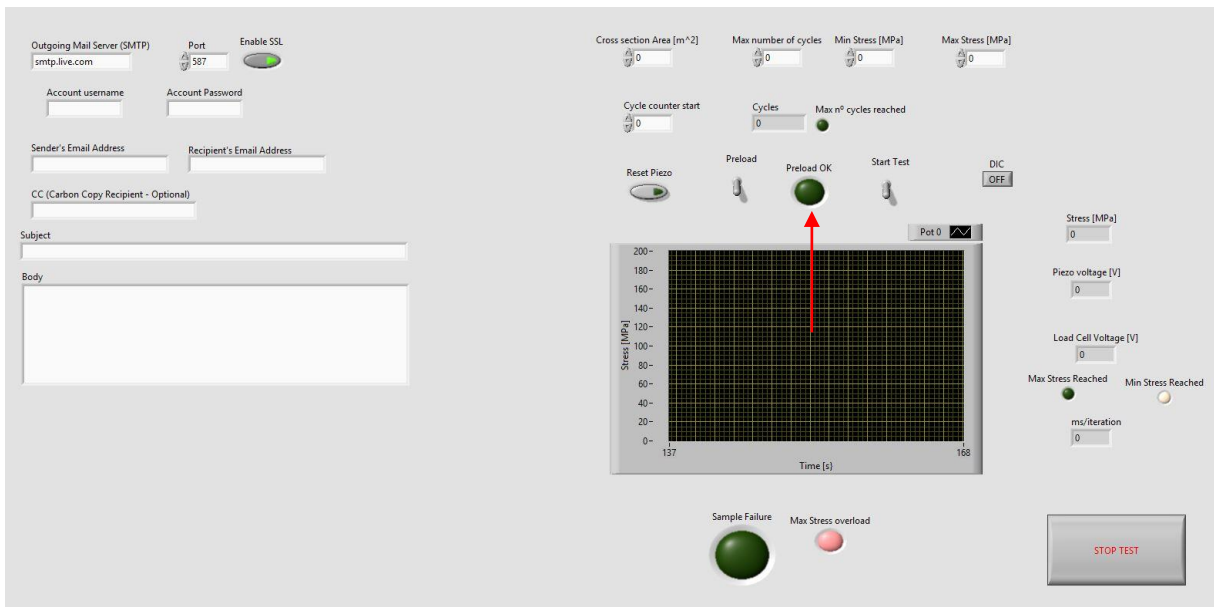
Program Set-up

1. Insert cross-sectional area (m^2);
2. Input min and max stress (MPa) and max number of cycles;
3. Optional: input email;
 - a. To receive email when specimen breaks;
 - i. Will receive stress, cycles, and time stamp;
4. Hit *PRELOAD*;

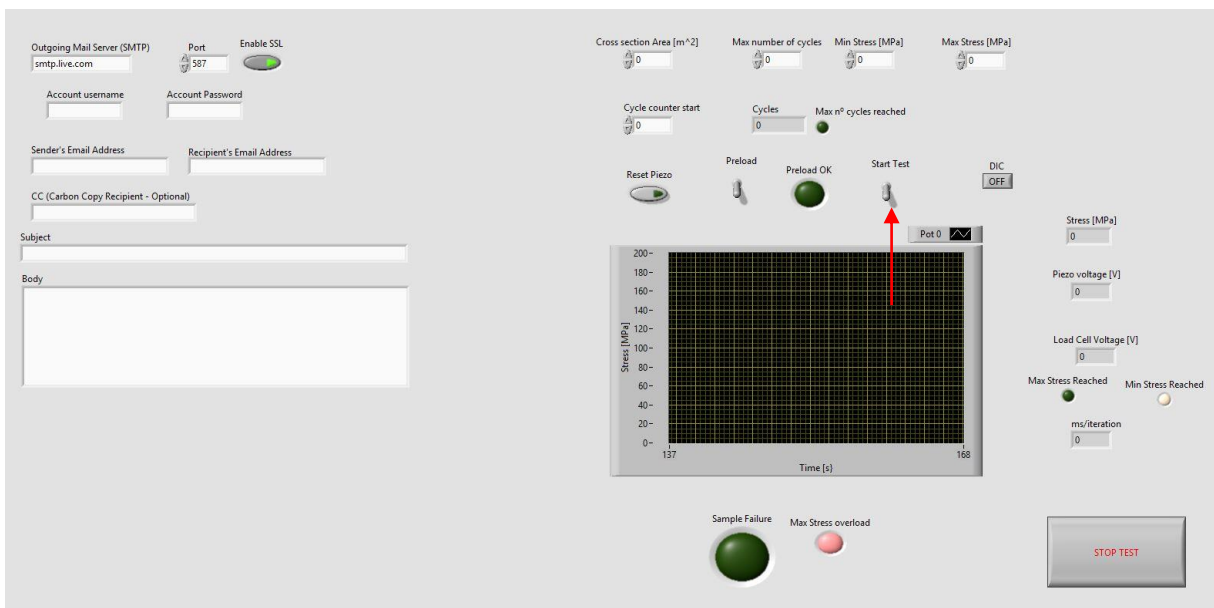


Fatigue testing machine development for microsample testing of Additively Manufactured Metals

a. Wait until pre-load ok light is lit;

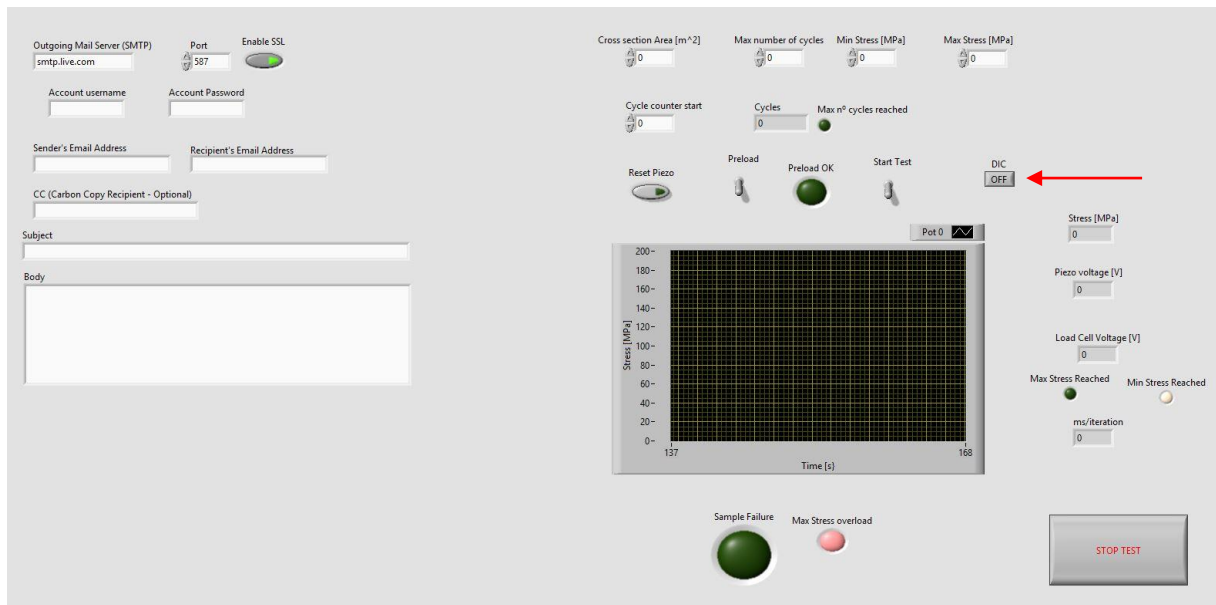


5. Once lit hit *START TEST*;



Running DIC mode

1. To run DIC mode press the *DIC* button;



- a. Communication is established with the DIC program once that program is running;
 - i. Serial communication parameters are pre-set and hardcoded on the program;
- b. To stop DIC mode press *DIC* button again;



Safety instructions



The moving parts of this system constitute no harm to the user.

Be careful while using, sharp edges present.

High voltage: some components use high voltage (up to 1000V), please read carefully the user's manual of each component for further safety instructions.

Air pressure system constitutes a risk of injury, use standard safety rules for this type of equipment.

If any damage is detected, do not turn on the system.